T.C.
NECMETTİN ERBAKAN UNIVERSITY
INSTITUTE OF SCIENCE

DEVELOPMENT OF NEW LOW pH ACTIVATABLE HYDRAZONE BASED NEAR-INFRARED REGION ABSORBABLE PHOTODYNAMIC THERAPY AGENTS

Ayşe İlayda BOYACI

MASTER'S THESIS

Department of Molecular Biology and Genetics

July -2025
KONYA

THESIS APPROVAL AND ACCEPTANCE

The thesis titled “Development of New Low pH Activatable Hydrazone-Based Near-Infrared Region Absorbable Photodynamic Therapy Agents” prepared by Ayşe İlayda BOYACI, has been accepted as a MASTER’S THESIS by the following jury on 03/07/2025 unanimously in the Department of Molecular Biology and Genetics of the Institute of Science at Necmettin Erbakan University.

Jury Members	**Signature**
Chair	
Prof. Dr. Mahmut Deniz YILMAZ	……..
Advisor	
Asst. Prof. Dr. Tuğba Nur ASLAN	……..
Member	
Assoc. Prof. Dr. Gülcihan GÜLSEREN	……..

Approved by the Institute of Science Administrative Board on …./…/20.. with the decision number ……..

Prof. Dr. Havvanur UÇBEYİAY
Institute Director

This thesis study was supported by TUBITAK-1002 with project number 123Z681.

THESIS APPROVAL AND ACCEPTANCE

Bu tezdeki bütün bilgilerin etik davranış ve akademik kurallar çerçevesinde elde edildiğini ve tez yazım kurallarına uygun olarak hazırlanan bu çalışmada bana ait olmayan her türlü ifade ve bilginin kaynağına eksiksiz atıf yapıldığını bildiririm.

DECLARATION PAGE

I hereby declare that all information in this document has been obtained and presented in accordance with academic rules and ethical conduct. I also declare that, as required by these rules and conduct, I have fully cited and referenced all material and results that are not original to this work.

Ayşe İlayda BOYACI

Tarih: 03.07.2025

ÖZET

YÜKSEK LİSANS TEZİ

DÜŞÜK pH İLE AKTİFLEŞEBİLEN HİDRAZON TEMELLİ YAKIN KIZILÖTESİ BÖLGEDE ABSORPLAYABİLEN YENİ FOTODİNAMİK TERAPİ AJANLARININ GELİŞTİRİLMESİ

Ayşe İlayda BOYACI

Necmettin Erbakan Üniversitesi Fen Bilimleri Enstitüsü

Moleküler Biyoloji ve Genetik Anabilim Dalı

Danışman: Dr. Öğr. Üyesi Tuğba Nur ASLAN

2025, 74 Sayfa

Jüri
Dr. Öğr. Üyesi Tuğba Nur ASLAN
Prof. Dr. Mahmut YILMAZ
Doç. Dr. Gülcihan GÜLSEREN

Fotodinamik terapi (FDT), onkolojik ve onkolojik olmayan hastalıkların tedavisinde geleneksel tedavi yöntemlerine alternatif bir yöntem olarak değerlendirilmektedir. Zararsız ışık, oksijen ve fotoduyarlaştırıcı bileşiğin birleşimiyle çalışan bir metottur. Zararsız ışık, oksijen ve ön ilaç olan fotoduyarlaştırıcı kombinasyonu ile çalışan bir yöntemdir. FDT' nin çeşitli kanser türlerinde, akne ve sedef hastalığı tedavisinde, antimikrobiyal yüzeylerde veya tedavilerde kullanımı desteklenmiştir. Fotoduyarlaştırıcı suda çözünürlüğü ve yakın kızılötesi (near-IR) ışığı absorplama özellikleri önemli ve arzu edilen özelliklerdir. Ayrıca, kanser hücrelerine özel olarak yönlendirilmiş fotoduyarlaştırıcı, sağlıklı dokulara zarar vermeden yalnızca kanser hücrelerini hedefleyerek tedavi güvenliğini artırabilir. Fotoduyarlaştırıcı düşük pH'lı kanser dokularına özgü olarak asidik ortamda aktive edilmesi, hedef dışı aktivasyonu engellemenin bir yoludur. Bu tez kapsamında, hidrazon bağları içeren, pH-duyarlı (düşük pH'ta aktive olan), yakın-IR absorplayan ve sulu ortamda çözünebilen BODIPY bazlı fotoduyarlaştırıcı tasarlanmış ve sentezlenmiştir. Beş yeni PS ön ilaç bileşiğinden ikisi iyot gibi ağır atomlar içermekte (**7 ve PB1**), diğer üçü ise ağır atom içermemektedir (**7H, PB1H, PB2H**). Ağır atom içeren 7 ve PB1'in çok daha etkili olduğu ve yüksek singlet oksijen kuantum verimlerine sahip olduğu belirlenmiştir. Fotoduyarlaştırıcı analizi sonrasında, hidrazon bağı içeren kafes yapılı **PB1**'in, aktive bileşik olan 7'ye kıyasla daha düşük aktivite gösterdiği belirlenmiştir. Bu nedenle, **PB1** düşük pH'ta aktive olan bir ön ilaç PS olarak kullanılabilir. Fotositotoksisite çalışmaları da MCF-7 insan meme kanseri hücre hattı üzerinde yapılan in vitro çalışmalarla başarıyla gerçekleştirilmiştir.
.

Anahtar Kelimeler: Aktifleştirilebilir Fotoduyarlaştırıcı, BODIPY, Fotodinamik Terapi, Kanser Tedavisi

ABSTRACT

MS THESIS

DEVELOPMENT OF NEW LOW pH ACTIVATABLE HYDRAZONE-BASED NEAR-INFRARED REGION ABSORBABLE PHOTODYNAMIC THERAPY AGENTS

Ayşe İlayda BOYACI

INSTITUTE OF SCIENCE NECMETTİN ERBAKAN UNIVERSITY
THE DEGREE OF MASTER OF SCIENCE

Advisor: Asst. Prof. Dr. Tuğba Nur ASLAN

2025, 74 Pages

Jury
Asst. Prof. Dr. Tuğba Nur ASLAN
Prof. Dr. Mahmut Deniz YILMAZ
Assoc. Prof. Dr. Gülcihan GÜLSEREN

Photodynamic therapy (PDT) is considered as an alternative method to traditional treatment methods in the treatment of oncological and non-oncological diseases. It is a method that works with a combination of harmless light, oxygen and prodrug photosensitizers (PS). PDT use has been supported in various types of cancer, treatment of acne, psoriasis and antimicrobial surfaces or treatments. Water solubility and near-IR absorption are important and desirable features of photosensitizers. In addition, photosensitizers specifically directed at cancer cells can increase treatment safety by targeting cancer cells without damaging healthy tissues. Activation of the PSs in the acidic medium is a method to inhibit off-target activation due to the low pH of the cancerous tissues. In this thesis, pH-sensitive (low pH-activating), near-IR absorbing, aqueous medium soluble BODIPY-based photosensitizers containing hydrazone bonds were designed and synthesized. Among the five new PS prodrug molecules, two of them are bearing iodine heavy atoms (**7** and **PB1**) and the other three are heavy-atom-free (**7H**, **PB1H**, **PB2H**). It was determined that heavy atom bearing **7** and **PB1** are much more effective and have high singlet oxygen quantum yields. After analysis of the PSs, it was determined that hydrazone bond bearing caged structure **PB1** has decreased activity compared to the activated molecule **7**. Therefore, **PB1** could be employed as a low pH-activating prodrug PS. The photocytotoxicity studies were also employed successfully using *in vitro* studies on MCF-7 human breast cancer cell lines.

Keywords: Activatable Photosensitizer, BODIPY, Cancer Therapy, Photodynamic Therapy

ACKNOWLEDGMENT

I would like to respectfully thank Asst. Prof. Dr. Tuğba Nur ASLAN, who accepted me as her student, for her valuable scientific contributions and efforts.

I would like to sincerely thank my co-advisor Assoc. Prof. Dr. Yusuf ÇAKMAK for giving me the opportunity to develop myself as a master student and for trusting me to carry out a 1002 project for my thesis study. I am also grateful for his guidance and patience throughout this journey.

I would like to thank my dear lab mates Beyza BAŞAR, who suffered with me on this journey, my moral supports Aliye Beyza ÖZÇELİK, Betül ALTUNKAYNAK, Ravza UÇAR, Emin ŞAHİN.

I would also like to express my thanks and best wishes to dear Prof. Dr. Mahmut Deniz YILMAZ who helped everyone in our laboratory.

I would like to thank my dear family for all their support and best wishes.

Lastly, I would like to thank my beloved husband for his moral support. Whenever I felt like failing, he helped me stay strong

Ayşe İlayda BOYACI

KONYA-2025

CONTENTS

SYMBOLS AND ABBREVIATIONS

Symbols

mL: milliliter

μL: microliter

μM: Micromolar

mM: Millimolar

MHz: Mega Hertz

$^1O_2$: Singlet oxygen

Abbreviation

aPS: Activatable Photosensitizer

ATP: Adenosine Triphosphate

$BF_3.OEt_2$: Boron trifluoride diethyl etherate

BODIPY: Boron-Dipyrromethene

DCM: Dichloromethane

DCE: Dichloroethane

DMSO: Dimethyl Sulfoxide

DMF: N,N-Dimethylformamide

DPBF:1,3-Diphenylisobenzofuran

EtOH: Ethanol

EtOAc: Ethyl Acetat

Net_3: Triethylamine

FRET: Fröster Energy Transfer

HpD: Hematoporphyrin Derivative

ISC: Intersystem Crossing

K2CO3: Potassium carbonate

MCF-7: Michigan Cancer Foundation-7 Cell Line

MeOH: Methanol

MeCN: Acetonitrile

MTT: 3-(4,5-Dimethylthiazol-2-yl)-2,5-Diphenyltetrazolium Bromide

N2: Nitrogen Gas

NaOH: Sodium Hydroxide

NIR: Near-Infrared Region

NMR: Nuclear Magnetic Resonance

PBS: Phosphate-Buffered Saline

PEG: Poly(ethylene glycol)

PET: Photoinduced Electron Transfer

PDT: Photodynamic Therapy

$POCl_3$: Phosphorus Oxychloride

PS: Photosensitizer

QTOF-LCMS: Quadrupole Time-of-Flight Liquid Chromatography–Mass Spectrometry

ROS: Reactive Oxygen Species

S0: Singlet Ground State

T1: Triplet State

TFA: Trifluoro Acetic Acid

THF: Tetrahydrofuran

TLC: Thin Layer Chromatography

TME: Tumor Microenvironment

UV: Ultraviolet

1. INTRODUCTION

Cancer is one of the lethal diseases that humans face and the disease rate is increasing year by year. The latest estimation about cancer cases reached 20 million new cancer cases in 2022 by the International Agency for Research on Cancer (IARC). Additionally, death rate of the cancer is also reached to 9.7 million. As the rate of diseases is gradually increasing, search for new therapeutic approaches is still being investigated. Currently, there are several treatments that show effects on cancer. These treatments can be listed as chemotherapy, radiotherapy, and immunotherapy. Although chemotherapy and radiotherapy aim to destroy cells, they do not discriminate between healthy and tumor cells during the process (Zafar et al. 2025)Therefore, destruction of healthy cells leads to high rates of side effects on patients.

Among the alternative cancer treatment methods, one example is light-based therapy known as photodynamic therapy (PDT). Although PDT can be referred to as cancer therapy, it can be applied in the treatment of non-cancerous diseases such as infections against bacteria and fungi, actinic keratosis (Hu 2014; Zane et al. 2014). The reason why PDT is categorized as a light therapy is that one of the main contributors of the therapy is light. In the mechanism of the therapy light is accompanied by molecule called photosensitizer along with molecular oxygen.

Main factor that PDT is coming forward over the conventional therapies is to have minimize adverse side effects and improve patient quality of life. One approach for minimizing side effects is the increasing target specificity on used photosensitizer. Targeting strategies are often based on the cellular and molecular differences between cancerous and healthy cells, such as the overexpression of certain receptors or proteins. In literature examples of such targeted photosensitizers are studied. Additionally, the unique characteristics of the tumor microenvironment (TME) can be exploited for selective delivery.

In this thesis, TME is considered as a main differentiation factor between healthy and cancer cells. It is known that cancer cells' tumor microenvironment (TME) has a moderately lower pH compared to healthy cells (Lin et al. 2019). In our study, we aim to synthesize pH-activatable BODIPY based PSs by incorporating hydrazone bonds in our molecules. Hydrazone bonds are known to be stable at neutral pH; however, this bond is prone to cleavage under acidic conditions. It is believed that by adding this moiety, specificity of PS towards to cancer cells will be increased. Additionally, triethylene glycol

units were incorporated to improve the water solubility of the molecules, and distyryl units were conjugated for near IR absorption.

2. LITERATURE REVIEW

2.1. History of Photodynamic Therapy

In modern times, there have been important developments in the use of light for therapeutic purposes. One notable example is the pioneering study conducted by Oscar Raab and Hermann von Tappeiner, which represents a significant milestone in the history of PDT. In 1900, Oscar Raab observed the effects of acridine-based dye by applying it to *Paramecium* cells along with the light. After 2 hours, *Paramecium* cells began to die; on the other hand, without light, acridine-based dye did not have any effect on cells (Correia et al. 2021) . Later, von Tappeiner extended the study with Jodlbauer and introduced the term “photodynamic action” (Mitton and Ackroyd 2005).

In PDT, there are three components found. These are photosensitizers (PS), light, and molecular oxygen(Lan et al. 2019). Individually, these components are non-toxic to cells; however, when the PS is activated by light in the presence of molecular oxygen, a series of photochemical reactions occur, leading to the formation of cytotoxic species known as reactive oxygen species (ROS) (Agostinis et al. 2011). Besides the role in PDT, ROS are also found in our healthy cells as a byproduct produce from cellular oxidative metabolism and have participate for several essential cellular functions including cell survival, cell death (Mattila et al. 2015; Wei et al. 2024). The key distinction between role in PDT and general cellular mechanisms is when excessive ROS production and accumulation at the target side, cancer cells cannot eliminate the high levels of ROS by the antioxidant defenses; therefore, they enter the cell death phase, which can be either apoptotic or necrotic.

Compared to other cancer treatments, the side effects of PDT are less. Also, it is known that cancer cells show less resistance against PDT. Moreover, by the ongoing research on PDT in recent years, it is revealed that PDT can be converted to more targeted therapy. To do so, different approaches exist such as the usage of nanoparticle delivery systems or designing of targeted PSs that activate in the tumorous region (Mfouo-Tynga et al. 2021a; Tavakkoli Yaraki, Liu, and Tan 2022).

2.2. Components of PDT

2.2.1. Photosensitizer

A photosensitizer (PS) is a molecule that produces ROS through interaction with oxygen when exposed to a specific wavelength of light. There are some criteria for PS to apply for clinical purposes. These criteria can be listed as (Abrahamse and Hamblin 2016; Allison and Sibata 2010):

- Ideal PS should accumulate in the target tissue.
- Ideal PS should have low toxicity in the absence of light (low dark toxicity).
- It should have a high absorption peak within the therapeutic window, ideally in the near-infrared region (600-800 nm).
- It should have a high quantum yield for generating $^1O_2$ or ROS and exhibit high cytotoxicity when exposed to light.
- Synthesis and purification process of ideal PS should be easy

Throughout history, various photosensitizers have been developed, and they are categorized under three generations (Mfouo-Tynga et al. 2021b). Examples of first-generation PSs are hematoporphyrin derivative (HpD), that is synthesized from acid reaction of hemoglobin, and photofrin II, that is the purified version of HpD. HpD consists of a mixture of mono and oligomeric porphyrins obtained (Calzavara-Pinton, Venturini, and Sala 2005) from the blood. Photofrin II is clinically approved for the treatment of several pre-cancerous lesions and malignancies (Hamblin 2020).

Despite their extensive study, first-generation PSs have some significant drawbacks. Their synthesis and purification processes are challenging, they exhibit low photostability in the red region, and they can cause prolonged skin photosensitivity and have low water-solubility (Mfouo-Tynga et al. 2021c; Yu et al. 2022; Zhang et al. 2018) . To overcome these limitations, second-generation PSs were developed including methylene blue, bacteriochlorin, rose bengal, and phthalocyanines.

On the contrary of HpD, these PSs are pure rather than a mixture and they are known to have better tissue penetration due to activation by longer wavelengths. Third-generation PSs were developed to enhance specific localization of the PSs which was a common problem in the second-generation PSs.

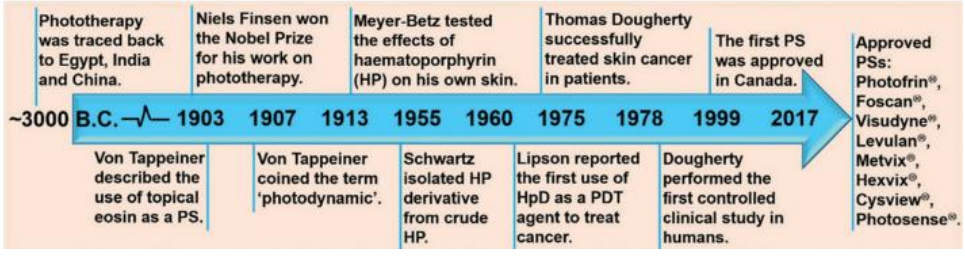

Figure 2.1. Timeline of development of PDT (Awuah and You 2012)

2.2.2. Light

Light is used for the activation of the photosensitizer, and the activated photosensitizer reacts with oxygen, leading to the production of radical species or $^1O_2$. When the PS is exposed to light, it absorbs energy from the wavelength and transforms from the singlet state to the excited singlet state. This excited state is not energetically stable, so some of the energy is released as fluorescence while the photosensitizer transitions to the excited triplet state. (Olszowy, Nowak-Perlak, and Woźniak 2023)The rest of the energy is then distributed through two additional pathways.

2.2.3. Molecular oxygen

Molecular oxygen is another component of PDT. With the activation of PS with the proper wavelength of light reacts with molecular oxygen to produce cytotoxic products. Molecular oxygen is also one of the limiting factors that affect the efficiency of therapy (Gunaydin, Gedik, and Ayan 2021). The microenvironment of a tumor is not equally same in the case of the level of molecular oxygen due to aggregation of massive amount of cancer cells (Zane et al. 2014). The vascular system is affecting the amount of molecular oxygen. Type of tumor also affects the efficiency of PDT. As is known in solid tumors, they have an oxygen-deprived microenvironment which leads to a limitation.

2.4. Mechanism of PDT

In the mechanism of PDT, PS is excited or activated by the specific wavelength of light and this activation leads to conversion of PS singlet ground state (S0) to short lived excited singlet state (S1) (Allison and Moghissi 2013). Later, the S1 state can go back to its original form by the emission of absorbed energy in the form of fluorescence or dissipated in the form of heat. However, it is possible to convert the S1 state to longer lived triplet state (T1) by the inter system crossing (ISC) which is a pivotal step for effective PDT. Jablonski diagram exhibits molecular photophysics by showing electronic states and energy transfers happening between states (Figure 2.2) (W. Li et al. 2022)

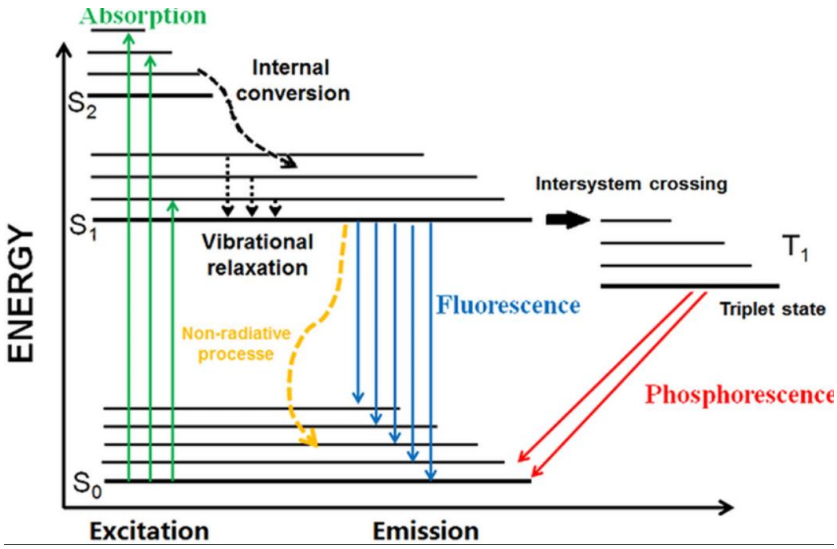

Figure 2.2. Jablonski diagram (Schweizer, Kubach, and Koch 2021)

After the formation of T1 state, there are two reactions that can take reactions can occur, both of which are responsible for generating cytotoxic species. In type I reaction, when a PS is excited with a specific wavelength, it interacts with surrounding biomolecules or substrates to form free radicals, such as hydrogen peroxide, and after that these free radicals react with the oxygen leading to formation of reactive oxygen species (Robertson, Evans, and Abrahamse 2009). Due to the non-requirement of oxygen, type I reactions are more suitable for hypoxic conditions in cancer (Z. Li et al. 2023)

In type II reactions, instead of interacting with biological substrates, PS directly react with molecular oxygen and leading the singlet oxygen ($^1O_2$) formation. The efficiency of PDT depends on depends not only on the amount of $^1O_2$ but also the location of its production. It is crucial production of $^1O_2$ at the target site, due to the short half-life of $^1O_2$. (Calin and Parasca 2006).

2.5. Effects of PDT on Cancer Cells

Cancer cells can uncontrollably proliferate due to several reasons. In normal conditions, cells can control their production mechanisms, however, intrinsic or extrinsic conditions can cause cancer cells to form. As cancer cells exhibit specific hallmarks that characterize their behavior, there are various strategies to eliminate cancer and destroy cancer cells by targeting and inhibiting these properties.

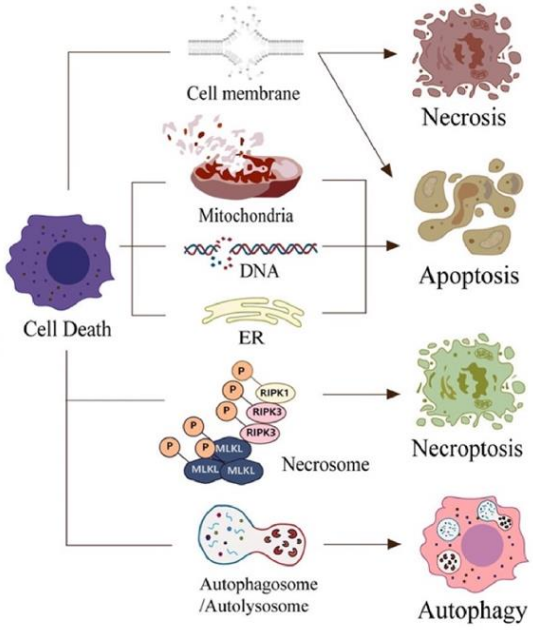

Figure 2.3. Illustration of cell death pathway caused by PDT (Singh et al. 2024)

PDT is one of the therapeutic approaches for cancer cell eradication and can induce different cell death mechanisms (Figure 2.3). One of the major cell death mechanisms that occurs in PDT is referred to as apoptosis. Apoptotic cell death describes as programmed cell death which characterized by shrinking of the cell while integrity of plasma membrane is intact for a while (Castano, Demidova, and Hamblin 2005). In addition to apoptosis, necrotic cell death can be observed in PDT.

Unlike apoptosis, necrosis is characterized by the disruption of plasma membrane integrity, resulting in the uncontrolled release of intracellular components into the surrounding environment (Fink and Cookson 2005). In general, it is believed that lower doses of PDT lead to more apoptotic cells, while higher doses lead to proportionately more necrotic cells (Robertson, Evans, and Abrahamse 2009). Cell death pathway occurs depends on several parameters such as type of cell and PS, cellular localization, light dose, oxygen partial concentration (Singh et al. 2024). Furthermore, PDT can cause damage to the vascular system of cancer tissues, leading to deprivation of nutrients and oxygen. Lastly, PDT has been shown to induce immunogenic cell death (ICD), which can stimulate an anti-tumor immune response (Lovell et al. 2010).

2.6. BODIPY

The first BODIPY (4,4-difluoro-4-bora-3a,4a-diaza-s-indacene) was synthesized in 1968 by Treibs and Kreuzer (Squeo et al. 2017). BODIPY is an organic dye and its derivatives are currently used in various applications including organic light-emitting device (OLED), bioimaging and sensor, a PS for photodynamic and photothermal therapy (Figure 2.4).

The excellent properties of BODIPY have garnered significant attention in research. These properties are listed as: excellent photophysical and chemical properties, high fluorescence quantum yield, easy tunability on the structure, and remarkable stability (Rybczynski et al. 2021).

Besides having excellent photophysical and photochemical properties, parent BODIPY dyes are not suitable for efficient PDT. Due to the highly fluorescent nature of the structure, the efficiency of intersystem crossing (ISC) has been insufficient to generate adequate amounts of singlet oxygen $^1O_2$ (Agazzi et al. 2019). To enhance ISC and increase production of $^1O_2$, heavy atoms such as iodine and bromide can be integrated into the structure. This process is named as heavy atom effect. One of the early examples of halogenated BODIPY molecules was given by Yogo and colleagues in which they were able to incorporate two iodine atoms to 2,6- position of the BODIPY core to enhance ISC and achieve a corresponding increase in $^1O_2$ production (Yogo et al. 2005). However, integration of halogen atoms into the molecules could enhance the dark toxicity (Turksoy, Yildiz, and Akkaya 2019).

Although most of the BODIPY structures exhibit hydrophobic characteristics which can be advantageous for cell membrane penetration (Kowada, Maeda, and Kikuchi 2015; Schad et al. 2025), in the case of clinical trials, hydrophobicity characteristics might cause problems. For the efficient distribution of the dye molecules in the systemic circulation, a drug must have certain solubility in the aqueous environment. To accomplish enhancement of water solubility of BODIPY molecules, introducing side groups such as ethylene glycol units or loading PS into water-soluble micelles can be a solution to this problem.

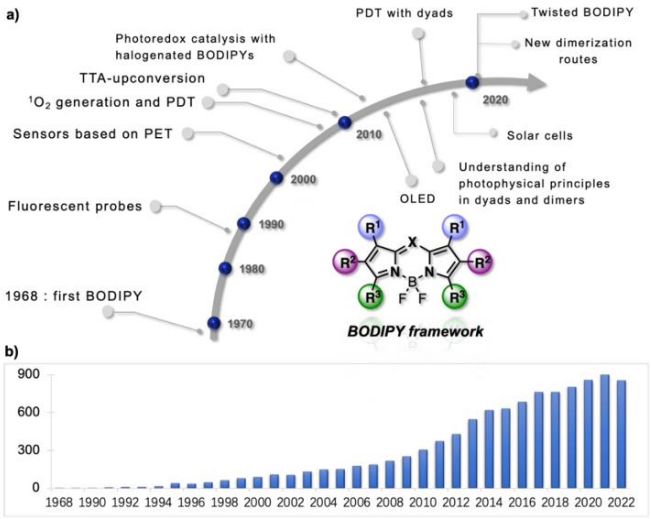

.

Figure 2.4. a) Development of BODIPY throughout the years in different applications b) Annual publications on BODIPY retrieved from Scifinder(Wang et al. 2023).

2.7.Hydrazone Groups-Dynamic Covalent Bonds

Dynamic covalent chemistry is a concept of including reversible reactions that take place under certain circumstances (Rowan et al. 2002). Hydrazone groups are one of the members of dynamic covalent bonds which have C=N bond in their structure.

Hydrazone groups have inspired applications in a wide range of areas, including medicinal chemistry and supramolecular chemistry (Tatum, Su, and Aprahamian 2014). Hydrazone groups can be used in drug delivery systems. One goal of drug delivery system is that it activates or releases the drug at the target site, thereby minimizing uncontrolled drug release and reducing side effects.

Due to rapid or slow hydrolysis of hydrazone groups under mildly acidic conditions, hydrazone groups are widely used in drug delivery system for bacterial infections and cancer (Yoshida et al. 2013). Therefore, hydrazone groups can be integrated with the drugs via employing in a different drug delivery vehicle. Figure 2.5 indicates the functional groups of hydrazone structure. Formation of hydrazone bonds can be accomplished by three different mechanisms. One of the ways is the condensation of hydrazine or hydrazide with ketones or aldehydes (Sonawane, Kalhapure, and Govender 2017).

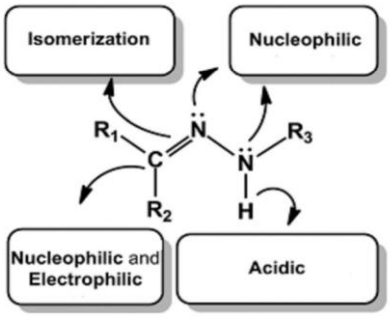

Figure 2.5. Structural configuration of hydrazone group (Sonawane, Kalhapure, and Govender 2017)

As the hydrazone bonds have popularity in the drug delivery system, Vendrell et al. reported the conjugation of BODIPY with a cytotoxic drug via hydrazone bond. The role of the hydrazone bond is the activation of pro-drug in macrophages M1 cell under acidic conditions (Fernandez et al. 2017). Figure 2.6 indicates the mechanisms of action of conjugated BODIPY fluorophore with a cytotoxic drug called doxorubicin.

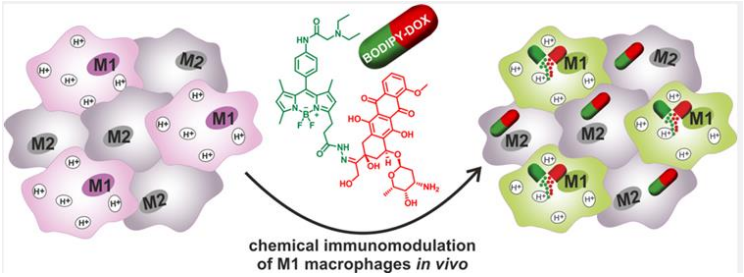

Figure 2.6. Mechanism of action of the activatable PS (Fernandez et al. 2017)

2.8.Activatable Photosensitizer

One of the essential goals in PDT is to increase the therapeutic selectivity of the therapy therefore it aims to minimize damage to healthy cells. This goal represents a key characteristic of PDT and distinguishes it from conventional cancer treatments such as chemotherapy and radiotherapy. To achieve this selectivity, a comprehensive understanding of the structural features of cancer cells, along with their intrinsic and extrinsic mechanisms at the cellular level, is essential. Today, it is known that cancer cells exhibit different properties compared to healthy cells. By targeting these differences, both the selectivity and efficiency of the therapy can be enhanced, as non-target tissues remain unaffected by the treatment or minimally effected (Figure 2.7). For increasing efficiency of the treatment, it is preferable to activate PS at the target site because half-life of the $^1O_2$

is limited in aqueous solution and migration through the body is not suitable for the efficient therapy (X. Li et al. 2017).

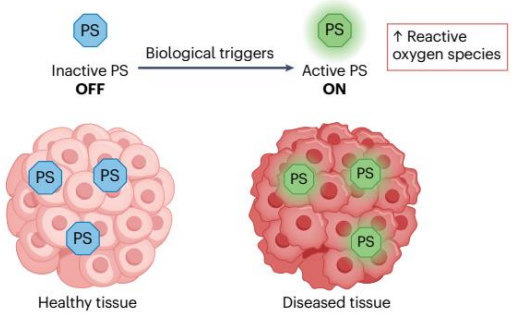

Figure 2.7. Illustration of general mechanism of activatable PS (Nestoros et al. 2024)

Activatable photosensitizers (aPS) are a promising approach for increasing the specificity of therapy. Mechanism of aPS relies upon the production of $^1O_2$ when aPS encounters a target of interest and after the exposure to light (X. Li et al. 2017).However, if target stimuli are not found, even if light is applied, no production of $^1O_2$ occurs. These targets can be receptors or biomolecules that are overexpressed in cancer cells such as glutathione, or they can be external conditions characteristic of the TME.

One of the examples for aPS is given by the Akkaya and coworkers which they target overexpressed glutathione in cancer cells(X. Li et al. 2017). In their study, they used BODIPY core in their molecule, and made modifications on it, such as the addition of water solubilizing moieties, to make molecules more soluble in physiological conditions. They used two Br ions on two sides of the BODIPY, to have heavy atom effects, and, they added quencher moieties which are responsive to glutathione. Quencher moiety is added to molecules to target glutathione. When PS is faced with the glutathione, quencher leaves the molecule, and by the irradiation of light, PS becomes active form and produces singlet oxygen (Figure 2.8).

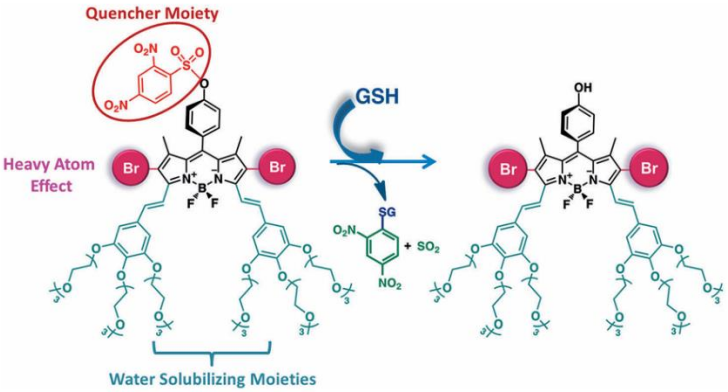

Figure 2.8. Mechanism of glutathione activatable PS (Turan et al. 2014)

2.8.1. pH dependence aPS

One of the unique features of the TME is that it has moderately lower pH. The reason is that cancer cells have uncontrollable proliferation, and to make it continuously they must have high energy consumption. At the cellular level ATP is the main energy source for every process (Bonora et al. 2012).

ATP can be generated through two main metabolic pathways: glycolysis and aerobic respiration. In normal cells, both types of processes are in the balance, and it is known that production of ATP is greater in the aerobic respiration. However, cancer cells generally lack oxygen, a so-called hypoxic condition due to the high number of cells to feed oxygen. To produce more ATP, cancer cells force themselves to process high rates of glycolysis rather than oxidative respiration, although oxygen is present in the environment and this phenomenon called Warburg effect (Kang et al. 2023). Lactic acid is produced as a byproduct in glycolysis and high amounts of lactic acid production leads to decrease in the pH of the environment (Liao et al. 2024). Therefore, the extracellular pH of cancer cells is typically around 6.0, whereas normal cells have a pH of about 7.4 (Lee, Shanti, 2021).

2.8.2. BODIPY based pH activatable PS

BODIPY molecule is another scaffold which could be used as a PS and one of the examples studied by Radunz et al. In their study, they were able to synthesize different BODIPY derivatives by sharing common phenolic groups at the meso position(Radunz et al. 2020). The purpose of these groups is the activation of PS at lower pH. Photoinduced electron transfer (PET) is used for the deactivation of S1 state and inhibits T1 state formation in healthy cells. However, in the acidic condition, the phenol group becomes

protonated and electronically decouples from the chromophore core, and this process results in the inhibition of the PET mechanism and leads to transition from S1 state to T1 state. Results exhibit that comparison on $^1O_2$ production under neutral and acidic conditions are different.

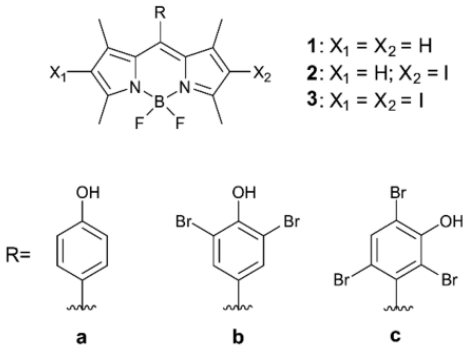

Figure 2.9 Activatable BODIPY-based PS. Reprinted with permission from: Radunz, S.; Wedepohl, S.; Röhr, M.; Calderón, M.; Tschiche, H. R.; Resch-Genger, U. J. Med. Chem. 2020, 63 (4), 1699–1708. Copyright 2020 American Chemical Society.

Another study is given by Çakmak and coworkers, they explored pH-activatable PSs where they synthesized three BODIPY-based photosensitizers. All PSs were included hydrazone units in their structures (Figure 2.10). One of the very first examples of incorporation of hydrazone bonds in PS were given in this research (Say et al. 2023). The inclusion of hydrazone units is successfully accomplished into BODIPY fluorophore, and three molecules are synthesized. In the APBOD1 molecule, the hydrazone units are attached at the 3-position of the BODIPY core, while in the APBOD2 molecule, the hydrazone unit is located at the 2-position. Results showed that the position of the inserted hydrazone bonds is affecting both quenching ability and production of singlet oxygen

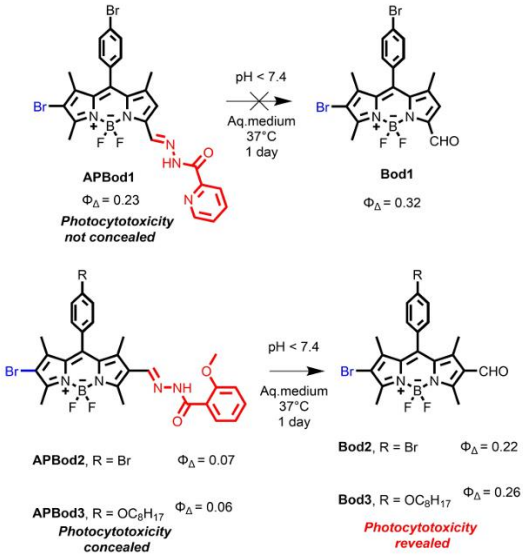

Figure 2.10. Photocytotoxic and caged molecules (Say et al. 2023)

In their further study, they developed pH-activatable bodipy based PS (Tatar et al. 2025). In that study, they were able to incorporate mono-styrl unit which absorption of PS has a bathochromic shift. This bathochromic shift is aimed at better skin penetration under optical window. By the addition of hydrazone bonds into the structure leads to the changing of singlet oxygen production. Also, in one of the molecules, two BODIPY molecules interact with each other through hydrazone linker. In this molecule, despite the qunecing mechanism that coming from the hydrazone linker, there is another mechanism called Fröster energy mechanism (FRET) that inhibit the singlet oxygen production even in the presence of light.

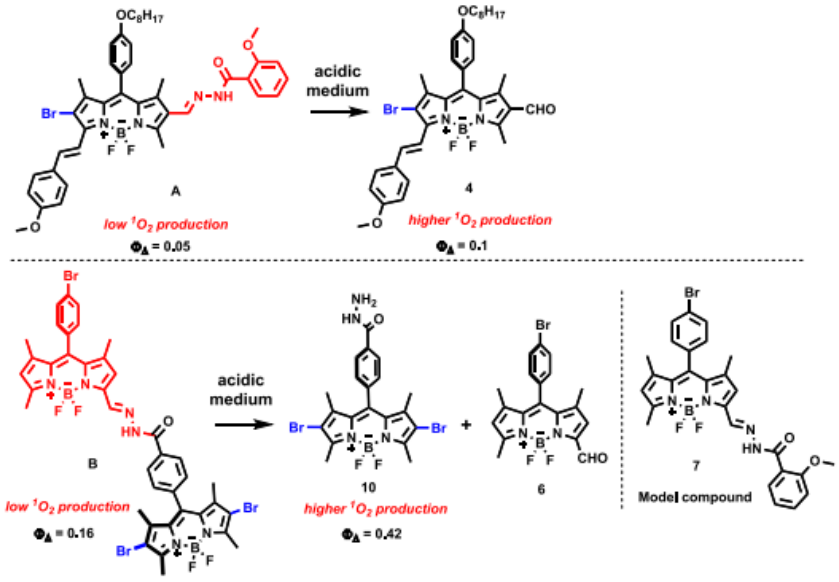

Figure 2.11. Hydrazone based pH activatable PS (Tatar et al. 2025)

3. MATERIALS and METHODS

3.1. Synthesize Steps of Designed Molecules

3.1.1. Synthesis of molecule 1

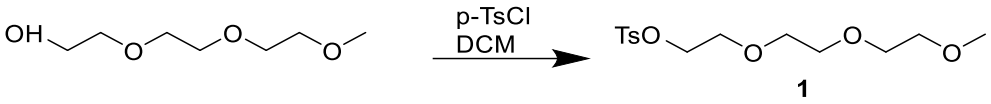

Figure 3.1. Synthesis step of molecule 1

3.158 mL triethylene glycol monomethyl ether (20 mmol, 1 eq.) is dissolved in 25 mL DCM. 5.7 g p-toluenesulfonyl chloride (30 mmol, 1.5 eq.) and 3.03 ml triethylamine (30 mmol, 1.5 eq.) were added (Krimalowski and Thelakkat 2019). Reaction is stirred at room temperature for 24 h. Column Chromatography was performed 1:5 Acetone: Hexane. 5,60 g product is obtained.

3.1.2. Synthesis of molecule 2

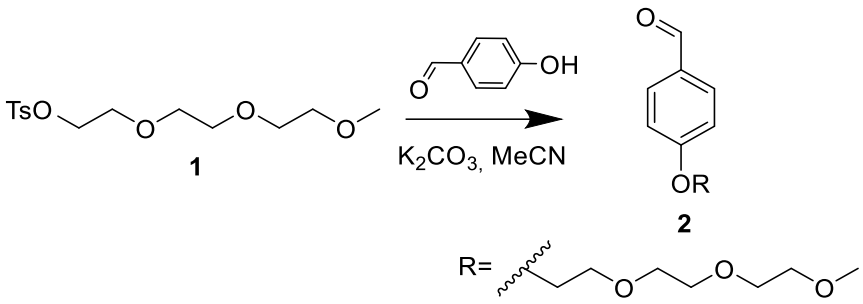

Figure 3.2. Synthesis step of molecule 2

647,2 mg of 4-hydroxybenzaldehyde (5,30 mmol, 1 eq) was dissolved in 70 mL DMF and 3,66 g of K_2CO_3 (26.5 mmol) is added to suspension. 2.5 g of **molecule 1** (6,89 mmol, 1.3 eq) was added to the mixture and the reaction was heated to 100 °C and stirred overnight under N2 atmosphere (Brunner and Gruber 2004). Water was added and the mixture was extracted with DCM. Column chromatography was done with 3%MeOH in DCM. 900 mg of product is obtained.

3.1.3. Synthesis of molecule 3

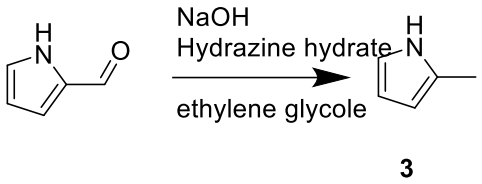

Figure 3.3. Synthesis step of molecule 3

For the synthesis of the **molecule 3** pyrrole-2-carboxaldehyde(6 g, 63.1 mmol), NaOH (13.2 g, 0.33 mmol), hydrazine hydrate (12.35 g, 39 mmo) is heated in 80 mL of ethylene glycol at 200°C under nitrogen for 3h (Ozdemir et al. 2022). In the reaction, a dean-stark trap is used to trap the formed molecule. The distilled part is extracted with diethyl ether and the organic phase is washed with deionized water, dried Na_2SO_4 and evaporated. 3.5 mL of pure product is obtained as a colorless oil.

3.1.4. Synthesis of molecule 4

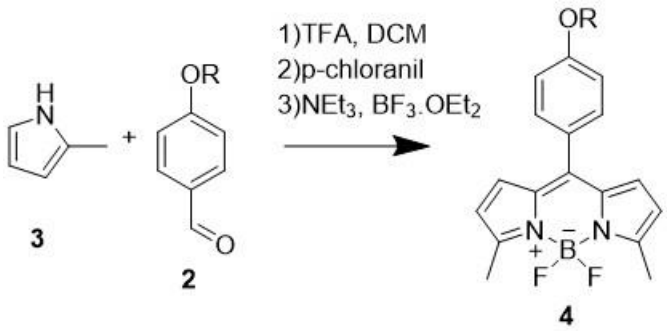

Figure 3.4. Synthesis step of molecule 4

Molecule 2 (0,745 mmol, 200 mg,1eq.), **molecule 3** (1,49 mmol, 120 mg, 2 eq.) and 2 drops of trifluoroacetic acid are dissolved in 15 mL dichloromethane (DCM) under nitrogen gas. Reaction is stirred at room temperature, under nitrogen gas overnight. Later, p-chloranil (0.745 mmol, 183 mg, 1 eq.) is added and stirred for 1.5 hours. 760 µL triethylamine and 760 µL boron trifluoride etherate are added and reactions stirred for 1.5 hours. Reactions are controlled with a 2% methanol-DCM system and reactions are completed and extraction is done three times water-DCM (3x100 mL). Purification is accomplished via column chromatography using a 2% methanol-DCM system. The product was obtained as 22.3 mg, yellow liquid. (0.048 mmol). ^{1}H NMR (400 MHz, $CDCl_3$) δ 7.46 (d, J = 8.7 Hz, 2H), 7.03 (d, J = 8.7 Hz, 2H), 6.76 (d, J = 4.1 Hz, 2H), 6.29

(d, J = 4.1 Hz, 2H), 4.26 – 4.21 (m, 2H), 3.96 – 3.90 (m, 2H), 3.81 – 3.77 (m, 2H), 3.75 – 3.72 (m, 2H), 3.72 – 3.67 (m, 2H), 3.60 – 3.56 (m, 2H), 3.41 (s, 3H), 2.67 (s, 6H). ^{13}C NMR (101 MHz, $CDCl_3$) δ 160.52, 157.03, 142.59, 134.51, 131.99, 130.26, 126.73, 119.18, 114.36, 71.96, 70.91, 70.71, 70.62, 69.64, 67.63, 59.08, 14.88. +APCI: C24H28BF2N2O4- calculated: 457.20450; found: 457.21157.

3.1.5. Synthesis of molecule 5

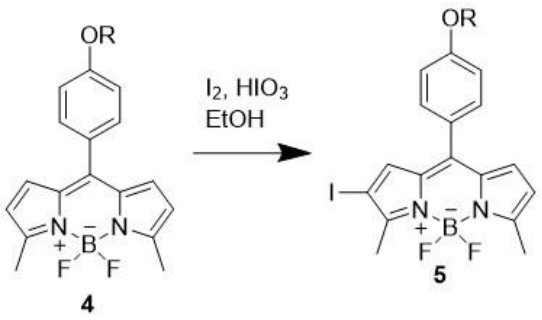

Figure 3.5. Synthesis step of molecule 5

Molecule 4 (0.436 mmol, 200 mg, 1 eq.) is dissolved in ethanol (64 mL). Iodine (0.130 mmol, 33.2 mg, 1 eq.) is added to the reaction and stirred. After the iodine is completely dissolved, iodic acid (HIO_3) (0.09 mmol, 16.87 mg, 0.22 eq.) is added and temperature is raised to 60°C. Reactions are controlled with TLC in a time interval and after 1 hour, reaction is completed. After the reaction was cooled to room temperature, 100 ml of DCM was added. Extraction was carried out by adding saturated sodium thiosulfate solution to the separatory funnel and DCM (3x180 mL). The obtained product was separated by silica gel column chromatography using 1% methanol-dichloromethane. 33 mg (0.056 mmol) of pure substance was obtained as orange precipitate. ^{1}H NMR (400 MHz, $CDCl_3$) δ 7.35 (d, J = 8.7 Hz, 2H), 6.95 (d, J = 8.7 Hz, 2H), 6.81 (s, 1H), 6.75 (d, J = 4.3 Hz, 1H), 6.27 (d, J = 4.3 Hz, 1H), 4.19 – 4.10 (m, 2H), 3.89 – 3.80 (m, 2H), 3.74 – 3.67 (m, 2H), 3.67 – 3.57 (m, 4H), 3.53 – 3.46 (m, 2H), 3.32 (s, 3H), 2.58 (d, J = 6.5 Hz, 6H). ^{13}C NMR (101 MHz, $CDCl_3$) δ 160.82, 159.32, 155.86, 142.04, 135.02, 132.01, 126.22, 120.58, 114.55, 71.97, 70.91, 70.71, 70.63, 69.61, 67.69, 59.08, 29.71, 15.23, 15.08. +APCI C24H27BF2IN2O4- calculated: 583.11248; found: 583.10821.

3.1.6. Synthesis of molecule 6

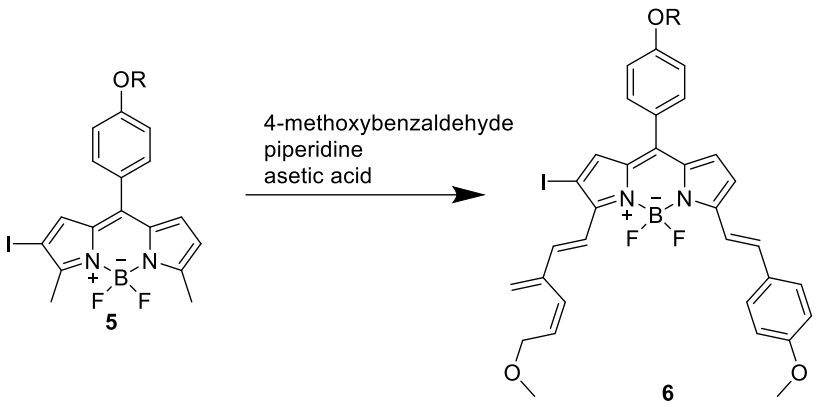

Figure 3.6 Synthesis step of molecule 6

Molecule 5 (0.045 mmol, 26.5 mg, 1 eq.) is dissolved in 10 mL benzene. 4-methoxybenzaldehyde (0.108 mmol, 14.82 mg, 2.4 eq.) is added to the balloon. Later, 500 µL piperidine and 500 µL acetic acid are added and the temperature is raised to 90°C. Dean-stark apparatus is used to collect benzene. Reaction is controlled via TLC. Extraction is done with water-DCM (3x90 mL). The obtained product was separated by silica gel column chromatography using 1% methanol-dichloromethane. 21 mg (0.0.025 mmol mmol) of pure substance was obtained. ^{1}H NMR (400 MHz, $CDCl_3$) δ 8.05 (d, J = 16.7 Hz, 1H), 7.70 – 7.55 (m, 6H), 7.44 (d, J = 8.8 Hz, 2H), 7.35 (d, J = 16.3 Hz, 1H), 7.04 (d, J = 8.8 Hz, 2H), 6.99 – 6.92 (m, 6H), 6.88 (d, J = 4.5 Hz, 2H), 4.26 – 4.17 (m, 2H), 3.95 – 3.90 (m, 2H), 3.90 – 3.84 (m, 6H), 3.82 – 3.75 (m, 2H), 3.73 – 3.66 (m, 4H), 3.60 – 3.54 (m, 2H), 3.39 (s, 3H). +APCI [C40H40BF2IN2O6+Na+], calculated: 843.18844; found: 843.17577.

3.1.7. Synthesis of molecule 7-7H

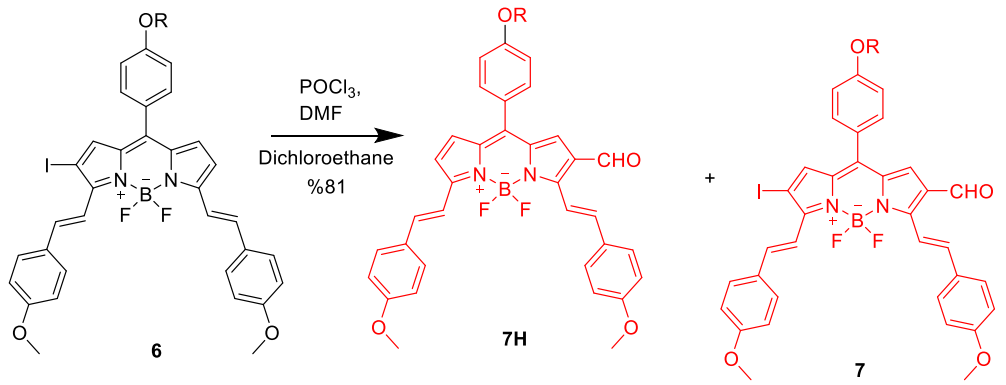

Figure 3.7. Synthesis step of molecules 7-7H

Firstly, 0.8 ml $POCl_3$ is dissolved in 10 mL DMF and stirred under nitrogen gas for 5 minutes at 0°C. Later, reaksion is warmed up to room temperature and stirred for 30 minutes. **Molecule 6** (0.058 mmol, 48 mg, 1 eq.) is dissolved in 10 mL dichloroethane and added to the reaction balloon. Reaction is stirred for 2 hours at 50°C. Saturated $NaHCO_3$ solution was prepared and added to the reaction in small fractions and the reaction was terminated after stirring for 1 hour. The obtained product was purified by prep tlc using 1% methanol-dichloromethane. The amount of product obtained was 20 mg (0.0276) belonging to the molecule 7H. As a minor product molecule 7 was obtained 1.3 mg (0.0015mmol). ^{1}H NMR (400 MHz, $CDCl_3$) δ 9.98 (s, 1H), 7.61 (d, J = 16.6 Hz, 2H), 7.57 (d, J = 8.9 Hz, 4H), 7.52 (d, J = 16.3 Hz, 1H), 7.41 (d, J = 8.9 Hz, 2H), 7.39 – 7.34 (m, 1H), 7.17 (s, 1H), 7.03 – 6.94 (m, 4H), 6.90 (d, J = 7.9 Hz, 4H), 4.20 – 4.12 (m, 2H), 3.86 (dd, J = 5.6, 4.0 Hz, 2H), 3.83 – 3.78 (m, 6H), 3.75 – 3.69 (m, 2H), 3.68 – 3.58 (m, 4H), 3.54 – 3.48 (m, 2H), 3.33 (s, 3H). ^{13}C NMR (101 MHz, $CDCl_3$) δ 194.63, 160.51, 159.65, 139.71, 138.84, 131.61, 131.07, 128.95, 128.49, 128.24, 127.67, 125.32, 113.74, 113.53, 113.29, 70.95, 69.90, 69.69, 69.61, 68.58, 66.72, 58.06, 54.45, 54.40. +APCI [C41H41BF2N2O7+H+], calculated: 723.29355; found: 723.30477.

^{1}H NMR (400 MHz, $CDCl_3$) δ 10.04 (s, 1H), 8.27 (d, *J* = 16.6 Hz, 1H), 7.76 – 7.68 (m, 2H), 7.68 – 7.62 (m, 5H), 7.47 (d, *J* = 8.8 Hz, 2H), 7.34 (s, 1H), 7.08 (d, *J* = 8.8 Hz, 3H), 7.03 – 6.92 (m, 5H), 4.28 – 4.22 (m, 2H), 3.97 – 3.91 (m, 2H), 3.88 (d, *J* = 3.1 Hz, 6H), 3.82 – 3.76 (m, 2H), 3.74 – 3.66 (m, 4H), 3.60 – 3.54 (m, 2H), 3.40 (s, 3H). ^{13}C NMR (101 MHz, $CDCl_3$) δ 185.43, 161.43, 161.21, 161.00, 141.32, 141.22, 140.72,

132.19, 131.64, 130.25, 129.81, 129.56, 129.31, 129.11, 125.97, 116.24, 116.21, 115.52, 114.93, 114.50, 114.38, 71.98, 70.93, 70.72, 70.65, 69.58, 67.80, 59.09, 55.48, 55.44, 30.94, 29.71, 29.67.

3.1.8. Synthesis of molecule PB1H

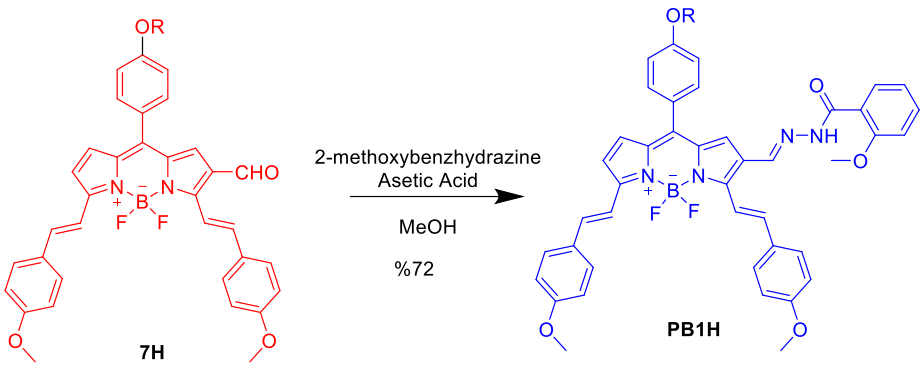

Figure 3.8. Synthesis step of molecule PB1H

Molecule 7H (0.017 mmol, 13 mg, 1eq.) is dissolved in 4 mL ethanol. 2-methoxybenzaldehyde (0.045 mmol, 7.47 mg, 2.6 eq.) and 1 drop of acetic acid are added to reactions. Reaction is stirred at 85°C and controlled with TLC. After terminating reactions, solvent is evaporated under low pressure. The obtained product tried to be obtained pure by silica gel column chromatography using 3% methanol-dichloromethane but it could not be obtained pure. Then the column system was changed to hexane: dichloromethane:ethyl acetate:ethanol (5:3:1:0.5). 15.3 mg of substance was obtained..^{1}H NMR (400 MHz, $CDCl_3$) δ 10.68 (s, 1H), 8.37 (s, 1H), 8.28 (dd, J = 7.9, 1.9 Hz, 1H), 7.70 – 7.56 (m, 6H), 7.51 – 7.45 (m, 3H), 9 7.39 – 7.30 (m, 2H), 7.20 (d, J = 16.6 Hz, 1H), 7.12 (t, J = 8.1 Hz, 1H), 7.04 (d, J = 8.8 Hz, 2H), 7.00 – 6.91 (m, 7H), 4.28 – 4.19 (m, 2H), 3.98 (s, 3H), 3.93 (dd, J = 5.7, 4.0 Hz, 2H), 3.90 – 3.83 (m, 6H), 3.83 – 3.75 (m, 2H), 3.76 – 3.63 (m, 4H), 3.62 – 3.52 (m, 2H), 3.40 (s, 3H). ^{13}C NMR (101 MHz, $CDCl_3$) δ 160.82, 160.05, 159.55, 159.42, 156.82, 156.04, 150.07, 141.87, 139.25, 137.73, 136.85, 132.23, 131.81, 131.07, 130.58, 128.74, 128.58, 128.14, 128.00, 127.93, 125.62, 125.01, 120.70, 119.63, 116.90, 115.78, 113.84, 113.70, 113.42, 113.30, 110.37, 76.31, 76.20, 75.99, 75.68, 70.95, 70.92, 69.88, 69.69, 69.60, 68.60, 66.68, 58.06, 55.15, 54.41. PB1H: +APCI: [C49H49BF2N4O8+H+], calculated 871.36843; found: 871.35493.

3.1.9. Synthesis of molecule PB1

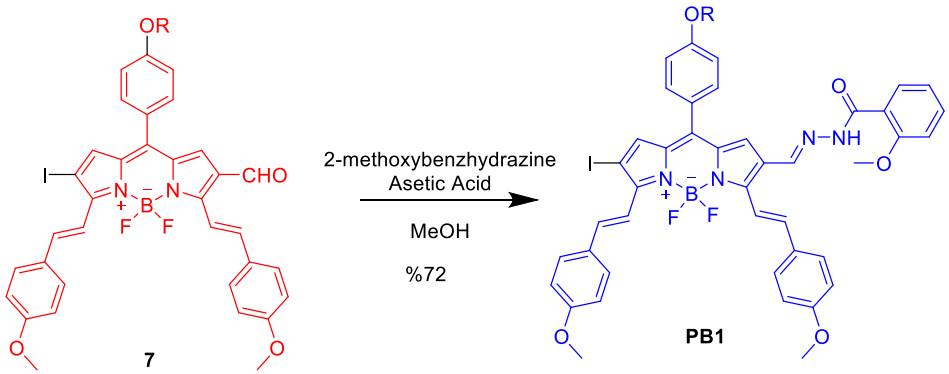

Figure 3.9. Synthesis step of molecule PB1

Molecule 7 (0.005 mmol, 5 mg, 1eq.) is dissolved in 2 mL ethanol. 2-methoxybenzaldehyde (0.017 mmol, 3 mg, 3 eq.) and 1 drop of acetic acid are added to reactions. Reaction is stirred at 85°C and controlled with TLC. After terminating reactions, solvent is evaporated under low pressure. Prep-TLC was used for the purification step by using MeOH-DCM (5%) solvent system. 2.7 molecule was obtained (0.0027 mmol). ^{1}H NMR (400 MHz, $CDCl_3$) δ 10.72 (s, 1H), 8.41 (s, 1H), 8.31 – 8.23 (m, 1H), 8.17 (d, J = 16.7 Hz, 1H), 7.70 – 7.58 (m, 6H), 7.54 – 7.43 (m, 3H), 7.41 (s, 1H), 7.32 (d, J = 16.4 Hz, 1H), 7.17 – 7.10 (m, 2H), 7.09 – 7.02 (m, 2H), 7.02 – 6.94 (m, 5H), 4.27 – 4.22 (m, 2H), 3.99 (s, 3H), 3.97 – 3.91 (m, 2H), 3.88 (d, J = 1.4 Hz, 6H), 3.81 – 3.76 (m, 2H), 3.76 – 3.67 (m, 4H), 3.61 – 3.56 (m, 2H), 3.40 (s, 3H). ^{13}C NMR (101 MHz, $CDCl_3$) δ 176.83, 172.47, 160.99, 159.95, 159.88, 159.79, 141.41, 141.40, 138.54, 138.34, 132.40, 131.85, 131.17, 131.15, 128.46, 128.43, 128.26, 125.23, 120.78, 120.42, 119.48, 113.85, 113.39, 113.36, 110.39, 70.95, 69.89, 69.69, 69.61, 68.57, 66.73, 58.06, 55.18, 54.43, 54.42, 41.48, 30.91, 28.68, 28.64, 28.34, 21.68, 13.10.

3.1.10. Synthesis of molecule PB2H

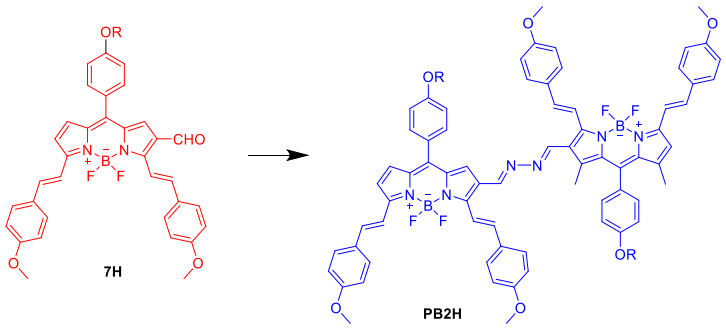

Figure 3.10. Synthesis step of molecule PB1

Molecule 7H (0.016 mmol, 12 mg, 1eq.) and hydrazine hydrate (0.007 mmol, 0.35 mg, 0.43 eq.) are dissolved in 4 mL dry methanol. 1 drop of acetic acid is added, and the reaction is stirred for 1 hour at room temperature. The reaction was completed by controlling TLC and evaporated under reduced pressure. Prep tlc was performed with 2% Methanol-DCM and 5.2 mg (0.0037 mmol) of green solid was obtained. ^{1}H NMR (400 MHz, $CDCl_3$) δ 8.88 – 8.79 (m, 2H), 7.71 – 7.57 (m, 12H), 7.50 (d, J = 8.8 Hz, 4H), 7.39 (d, J = 15.4 Hz, 4H), 7.30 (d, J = 6.3 Hz, 2H), 7.14 (s, 1H), 7.07 (s, 1H), 7.06 – 7.02 (m, 4H), 7.00 (d, J = 4.9 Hz, 2H), 6.98 – 6.91 (m, 8H), 4.26 – 4.19 (m, 4H), 3.96 – 3.89 (m, 4H), 3.87 (s, 12H), 3.81 – 3.74 (m, 4H), 3.74 – 3.63 (m, 8H), 3.61 – 3.52 (m, 4H), 3.38 (s, 6H). ^{13}C NMR (101 MHz, $CDCl_3$) δ 160.40, 148.26, 139.12, 132.10, 129.69, 129.09, 117.08, 114.64, 114.23, 71.94, 70.88, 70.68, 70.61, 69.61, 67.64, 59.08, 55.44, 53.44. +ESI: [C41H41BF2N2O7+Na]+: calculated: 745.28671, found: 745.28226.

3.2. Spectroscopic Measurements

After the synthesis of designed photosensitizers, molecules 7H, PB1H and PB2H were characterized as photophysical by measuring them in different solvents using absorbance and fluorescence spectrophotometers. The solvents used in these studies are dichloromethane (DCM), acetonitrile (MeCN), ethanol (EtOH), dimethyl sulfoxide (DMSO), tetrahydrofuran (THF).

For the fluorescence quantum yield experiment, zinc phthalocyanine is used as a reference molecule. Absorption and fluorescence spectroscopy were used. For fluorescence spectroscopy, molecules are excited at 650 nm.

3.2.1. Hydrolysis experiments

In this project, for the hydrolysis reaction experiment, molecules 7H, PB1H and PB2H were dissolved in DMSO: PBS buffer solution (4:1) by adjusting three different pHs (pH 7.4, 6, 5) and progress of the hydrolysis reaction were recorded by taking time-dependent spectroscopic measurements. For 7H, PB1H and PB2H molecule excitation wavelength is 600 nm in fluorescence spectroscopy.

3.2.2. Experiments on singlet oxygen production by chemical method

For the singlet oxygen production experiments, 1,3-diphenylbenzofuran (DPBF) is used as a trap molecule. DPBF is known to react with singlet oxygen and absorption of

DPBF at 410 nm is decreased according to interaction with singlet oxygen. This absorbance change allows quantitative analysis of singlet oxygen or reactive oxygen species (ROS) formation. DPBF were dissolved in dimethyl sulfoxide (DMSO), and molecules were dissolved in THF, and stock solution was prepared for each molecule. DPBF absorption peaks were set to near 1. Then 5uL of molecules and 5uL of DPBF were added to the quartz cuvette and MeCN was added to make up 3mL. For the testing there would be any decrease in the DPBF peak in the dark, up to 9 minutes, measurements were taken at the dark conditions. After that, light is applied to the molecules by applying LED (620 nm) distance from 60 cm to 5 seconds.

For the calculation of yield of singlet oxygen production, methylene blue was used as a reference molecule which is found in the literature. The same experimental set up was used during the measurements.

3.3. Cell Culture Experiments

3.3.1. MTT assay

To test the cytotoxic effects of molecules MTT assay is performed. Cancer cell line is selected as MCF-7 which is a human breast cancer line. 5000 cell/well were seeded to 96-well plate. After the incubation of cells, 7H, PB1H, and 7 molecules were administered to cells. For 7H and PB1H molecules between 0.5μM-32μM concentration were applied. For the molecule 7 and PB1 between 0.25μM-8μM concentrations were applied. Plates are divided into two groups: one of them is a dark group and the other one is a light group. 620 nm LED is applied to light group for 2 h, distance from 10 cm. After the light exposure, plates were kept under dark at the incubator 37 C for 24 h. After the one-day incubation, cells are treated with MTT. After 3 h from applying MTT, medium is discarded and DMSO was added to plates. Later, plates were incubated at incubator for 20 minutes. After the incubation time, absorbance measurements were taken for each well at ELISA Plate Reader at 490 and 570 nm.

4. RESULTS and DISCUSSIONS

4.1. Synthesize Steps of Designed Molecules

For the synthesis of the molecules, firstly triethylene glycol monomethyl ether molecule reacted with p-toluene sulfonic acid chloride and tosylated product 1 was obtained with 88% yield (Figure 4.1). Then, molecule number 1 reacted with 4-hydroxybenzaldehyde under Williamson ether synthesis conditions and molecule 2 was obtained with 63% yield.

To produce compound 3 (2-methyl pyrrole), pyrrole-2-carboxaldehyde was used as a precursor. In the presence of sodium hydroxide, hydrazine hydrate and ethylene glycol, compound 3 was obtained purely by distillation technique (with 67% yield) . This obtained substance was subjected to BODIPY formation reaction with aldehyde derivative (2). With a three-stage reaction, compound 4 could be obtained with 7% yield. Afterwards, molecule 5 could be obtained with 13% yield by monoiodination reaction. Using Knoevenagel reaction conditions, molecule 5 was reacted with 4 methoxybenzaldehyde and molecule 6 was obtained with 58% yield. In the next step, the formylization reaction of molecule 6 was carried out according to Vilsmeier-Haack reaction conditions. In this reaction, phosphorus oxychloride, dimethyl formamide and dichloroethane were used as solvents. It was determined that deiodination product 7H was obtained instead of molecule 7, which was expected to be obtained after mixing at 50°C for 2 hours. This finding made towards the end of the study seems quite interesting. Because no such dehalogenation reaction was found with this reaction in literature research. This unexpected reaction could not be predicted for this reason. In the last step, this halogen-free 7H molecule was used to obtain the molecule numbered PB1 and again the halogen-free PB1H molecule was obtained instead of the PB1 molecule as the product. In this reaction, the hydrazone bond was formed and 2-methoxybenzhydrazide, acetic acid and dry ethanol were used, and the final product was obtained with 72% yield. The second target product PB2H was again obtained with the 7H molecule, this time by reacting with hydrazine hydrate in dry ethanol and combining two BODIPY units with a condensation reaction and the product was obtained with 22% yield. After the necessary purifications, characterization, measurement and application studies of the molecules were carried out.

.

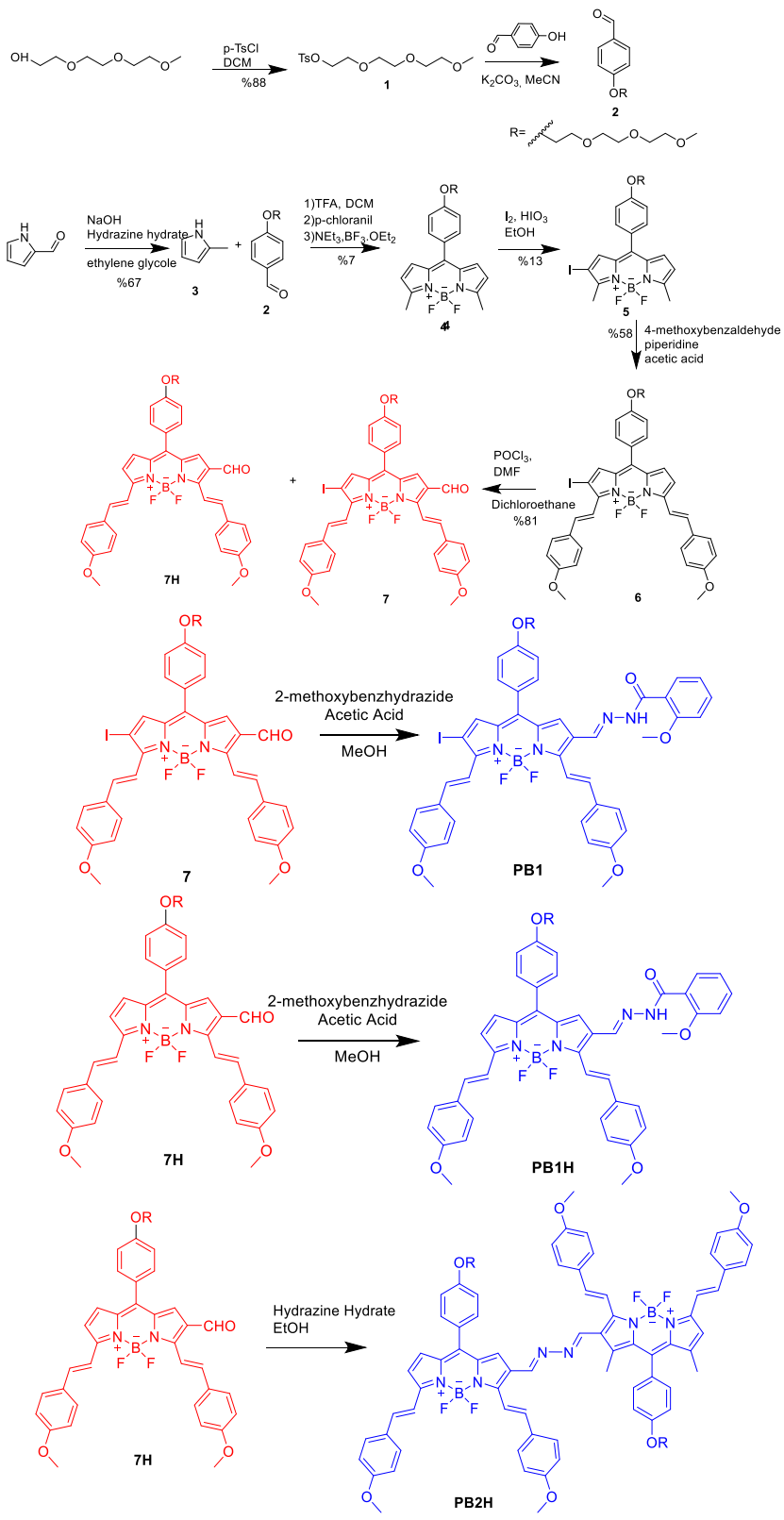

Figure 4.1. Synthesis steps of designed molecules.

4.2. Spectroscopic Measurements

4.2.1. Photophysical characterization

Measurements of photophysical characterization of molecule 7H, PB1H, and PB2H are taken in 5 different solvents (DCM, THF, DMSO, MeCN, EtOH). Although the solvents change, similar peak absorption is observed. For molecule 7H, the maximum absorption peak is obtained at 640 nm which is close to the near-infrared region compared to parent BODIPY molecule. It is known that general BODIPY molecules have an absorption peak at 500 nm. However, addition of the distyryl units at the position of 3-, and 5- leads to shifting of this peak to the near-IR region (bathochromic shift).

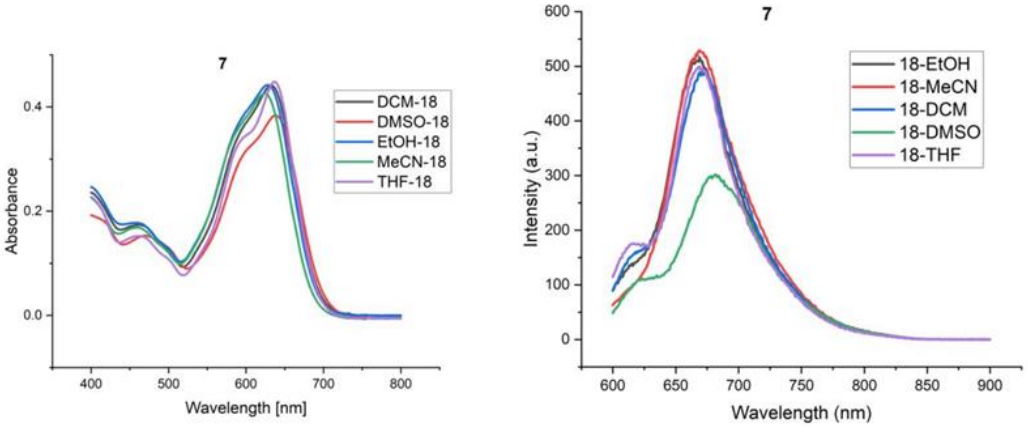

Figure 4.2. Absorbance and fluorescence graphs of molecule 7H ($1.7x10^{-5}$ M)

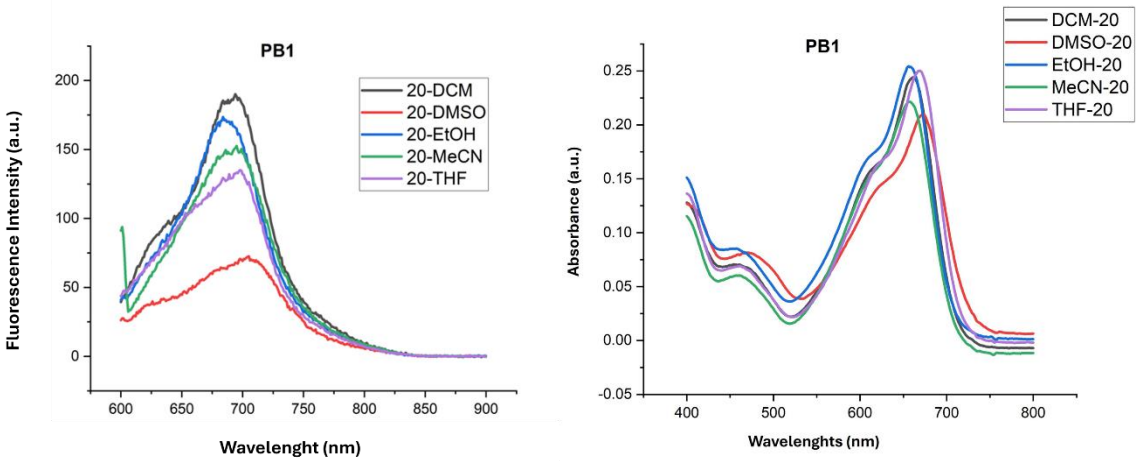

Figure 4.3. Absorbance and fluorescence graphs of molecule PB1H ($2.6x10^{-5}$ M).

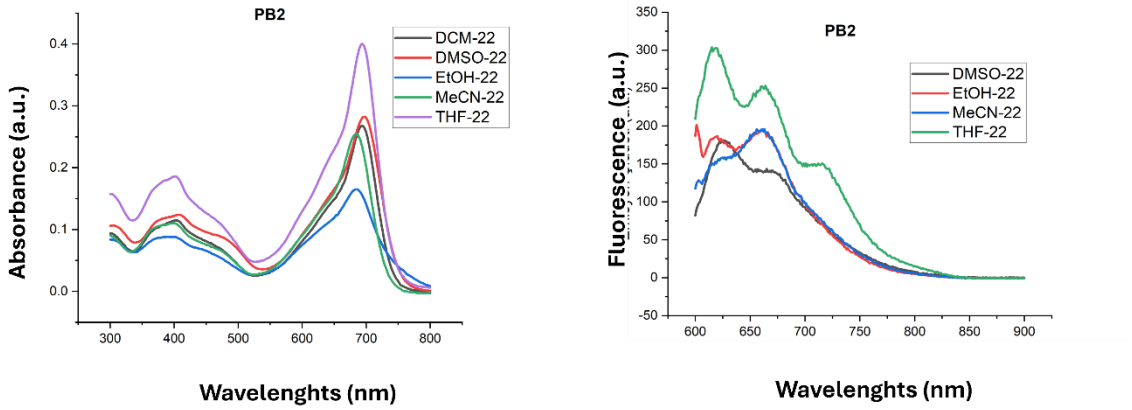

Figure 4.4. Absorbance and fluorescence graphs of molecule PB2H ($9.63x10^{-6}$ M).

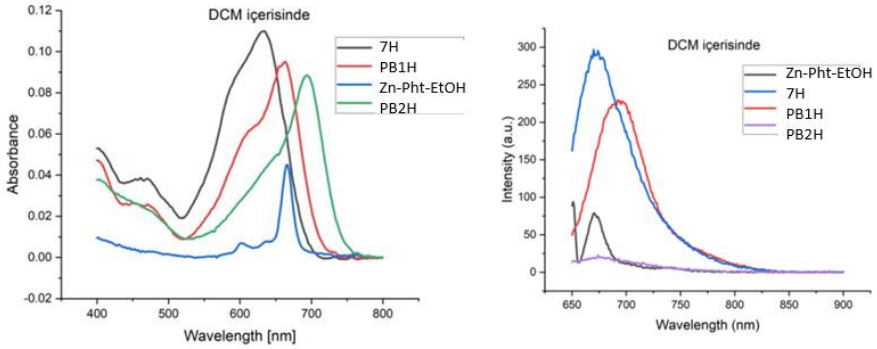

Figure 4.5. Absorbance and fluorescence graphs of molecules 7H, PB1H, PB2H.

4.2.2. Hydrolysis experiments

To understand the conversion of hydrazone unit the aldehyde groups, hydrolysis experiments were performed at different pH conditions. PB1H, and PB2H molecules are tested in DMSO: PBS (4:1) buffer system, and absorbance and fluorescence measurements were performed at 0, 1, 2, 24, 48 and 72 hours at pH 5, 6, and 7.4. It is expected that in acidic conditions hydrazone units will be hydrolyzed and converted to aldehyde groups. Absorption and emission spectrometers were used for these experiments.

Behavior of the molecule PB1H at the acidic and neutral pH corresponds to our expectation. Comparison of molecules 7H and PB1H shows that at neutral pH, absorbance and fluorescence peaks of PB1H did not change with time (Figure 4.6). On the other hand, at pH 6, that is, in a slightly acidic environment, it is observed that a clear change occurs depending on time, and the PB1H compound was converted to compound

7H (Figure 4.7). It was observed that there were significant changes, especially on the 24, 48 and 72 hours. Similar results were also seen at pH 5 (Figure 4.8).

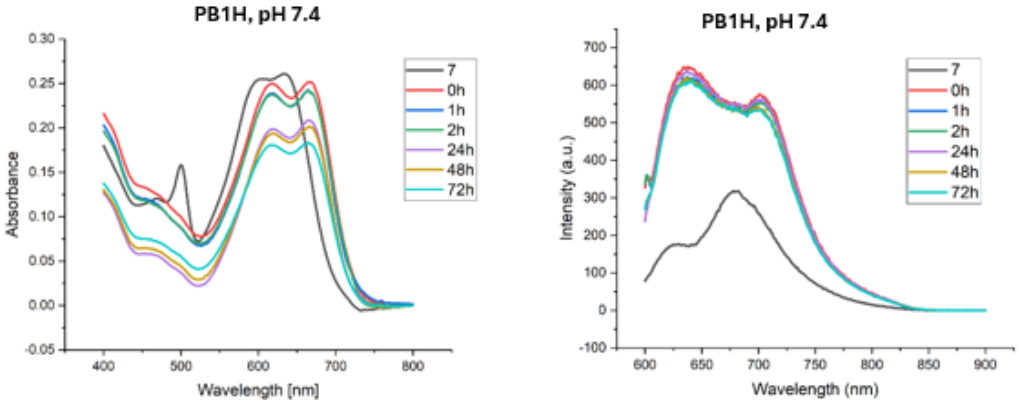

Figure 4.6. Hydrolysis of PB1H with time observed by the absorbance and fluorescence spectroscopy (at 37° C in pH 7.4 ($2.5x10^{-5}$ M) and compound 7H was also shown for comparison.

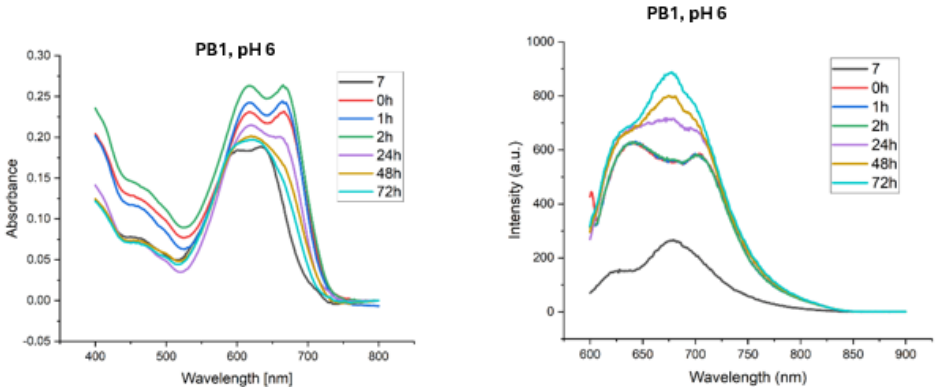

Figure 4.7. Hydrolysis of PB1H with time observed by the absorbance and fluorescence spectroscopy (at 37° C in pH 6 ($2.5x10^{-5}$ M) and compound 7H was also shown for comparison.

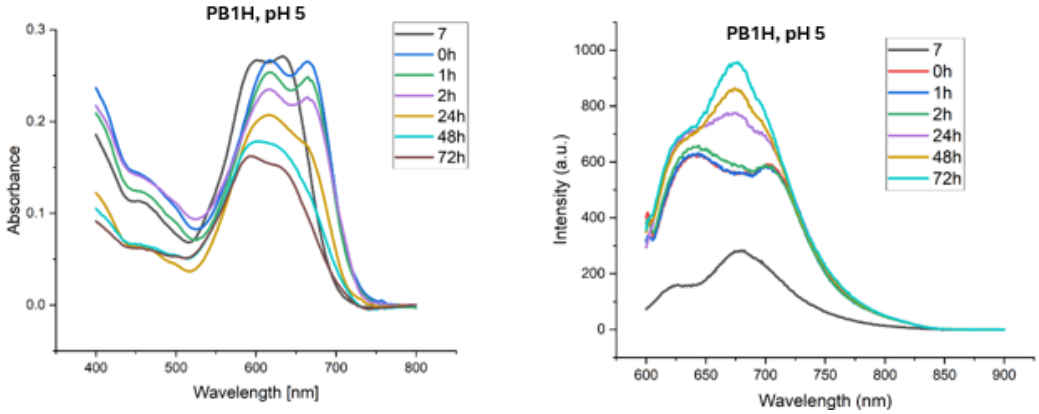

Figure 4.8. Hydrolysis of PB1H with time observed by the absorbance and fluorescence spectroscopy (at 37° C in pH 5 ($2.5x10^{-5}$ M) and compound 7H was also shown for comparison.

Hydrolysis experiments were also performed on PB2H molecules. PB1H and PB2H share a similar structure feature, as both bear hydrazone bonds. PB1H molecule is an acyl hydrazone derivative, while PB2H is a hydrazone derivative. Therefore, although the hydrolysis reactions of these compounds give similar results, that is, the same product is formed, differences in reaction kinetics can be expected. In the hydrolysis molecules were different results obtained for compound PB2H compared to the PB1H. As previously discussed, PB1H molecules are more resistant to change at the neutral pH, however, results show that PB2H molecule was more prone to hydrolysis in neutral pH conditions (Figure 4.9). Figure 4.10 and figure 4.11 exhibit observation at lower pH conditions and resulted as that the PB2H hydrolyzes rapidly in environments with pH values of 6 and 5. Thus, it was concluded that PB2H can be preferred when a faster hydrolysis reaction is desired and a release in less than 24 hours is required.

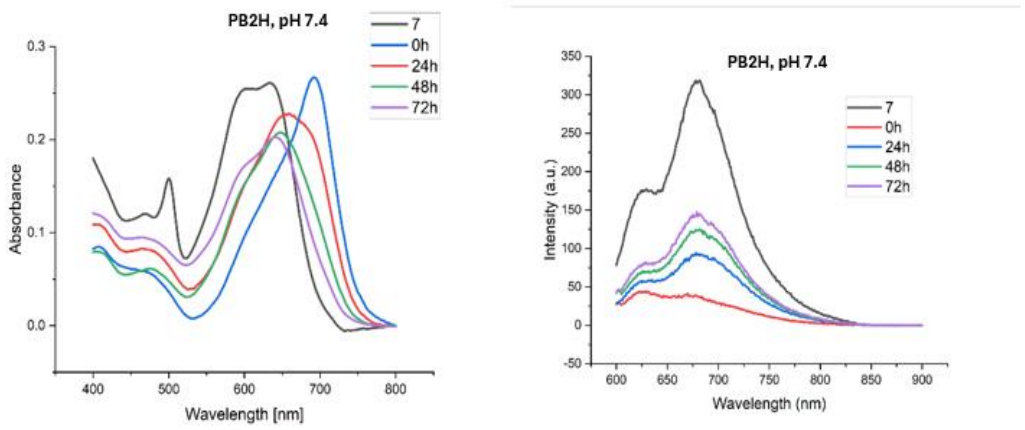

Figure 4.9. Hydrolysis of PB2H with time observed by the absorbance and fluorescence spectroscopy (at 37° C in pH 7.4 ($1x10^{-5}$ M) and compound 7H was also shown for comparison.

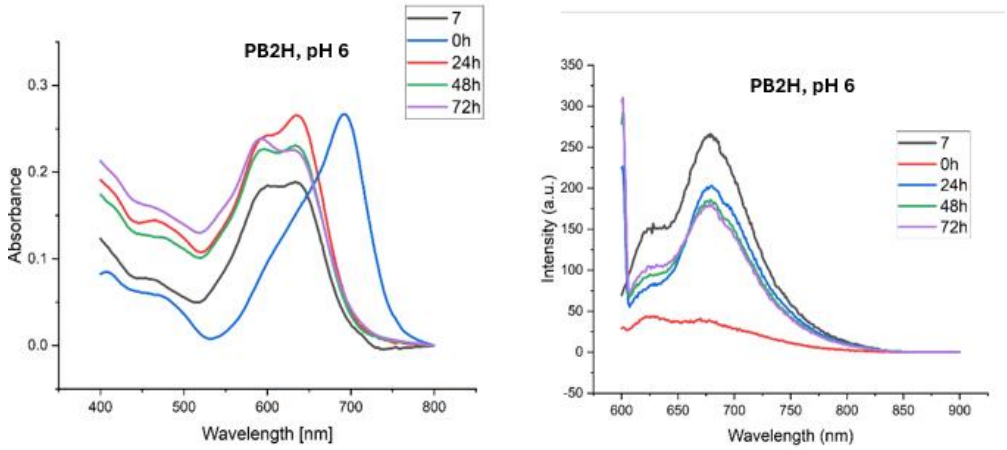

Figure 4.10. Hydrolysis of PB2H with time observed by the absorbance and fluorescence spectroscopy (at 37° C in pH 6 ($1x10^{-5}$ M) and compound 7H was also shown for comparison.

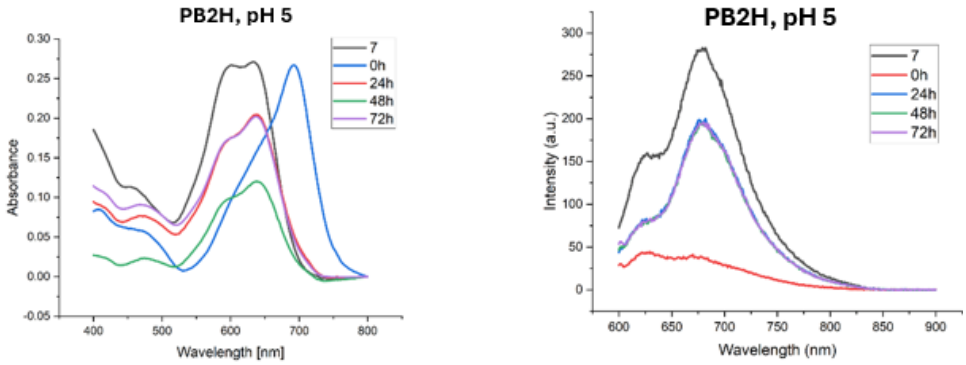

Figure 4.11. Hydrolysis of PB2H with time observed by the absorbance and fluorescence spectroscopy (at 37° C in pH 5 ($1x10^{-5}$ M) and compound 7H was also shown for comparison.

4.2.3. Experiments on singlet oxygen production by chemical method

For the understanding of the singlet oxygen production capacities of the molecules, experiments on singlet oxygen production were conducted. Since halogenated versions of hydrazone-based structures are expected to show better $^1O_2$/ROS forming ability, the results of the halogenated versions are shown here, namely 7 and PB1. Figure 4.12 shows the DPBF decreases for molecule 7. According to the results obtained we calculated the singlet oxygen quantum yield in comparison with the reference PS, methylene blue. The single oxygen production yields of the molecules were calculated as 0.35 and 0.26 for molecules 7 and PB1, respectively. This result indicates that the active form of the PS, 7 produces higher singlet oxygen/ROS compared to inactive form, PB1.

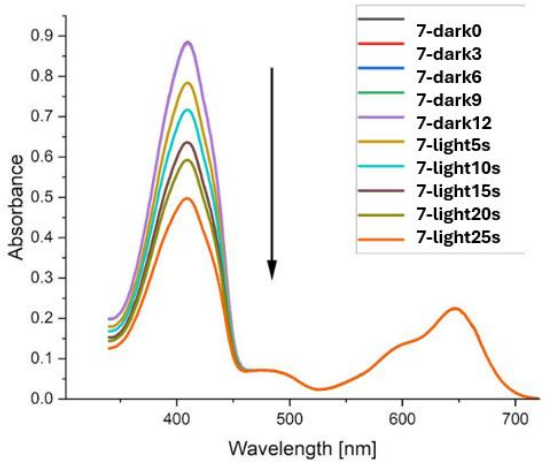

Figure 4.12. Singlet oxygen production measurement of molecule 7 (in MeCN).

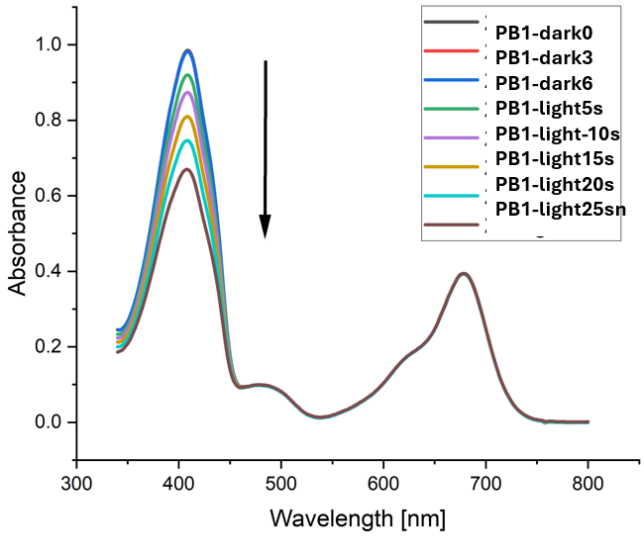

Figure 4.13. Singlet oxygen production measurement of molecule PB1 (in MeCN).

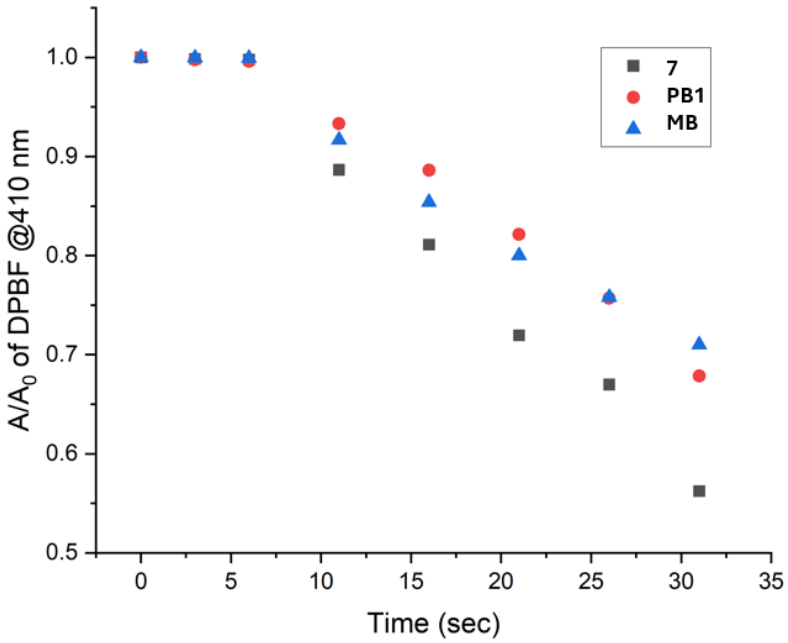

Figure 4.14. Time-dependent decrease in DPBF absorbance at 410 nm induced by photosensitizers.

4.3. Cell Culture Experiments

4.3.1. MTT assay

To test the cytotoxic effects of molecules on healthy and cancer cell line, MTT assay was performed for four molecules.

Figure 4.15 shows the effect of molecule 7H on MCF-7 cell line in dark group. According to the result, molecule 7H does not show dark toxicity. Despite this result, in

light group, a decrease was observed starting from the 1μM (Figure 4.16). The EC50 value for this molecule is estimated to be around 4 μM.

When compared to cell viability decreases between 7H and 7 molecules, 7H has lower efficiency as a PS due to the absence of heavy atom effect that coming from the iodine atom. The EC50 for 7H is estimated to be around 4 μM. We have also employed these experiments using the hydrazone-based structure PB1H. The EC50 for this compound under light irradiation is estimated as 4 μM (Figure 4.18). These results are in parallel with the results obtained using indirect formation of $^1O_2$/ROS using spectroscopic measurements. It shows that, caging of ROS formation is not possible for nonhalogenated hydrazone-based structures. This could be due to the lower ROS formation, even in the active form, and the difference could be minimum, or some other pathways (type I ROS formation) may have been followed. The latter may have been involved in more complex mechanisms, which are beyond the focus of the current study.

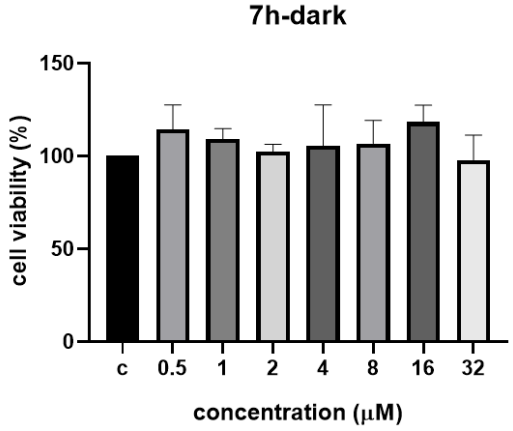

Figure 4.15. MCF-7 Cell viability assay results for molecule 7H in dark group.

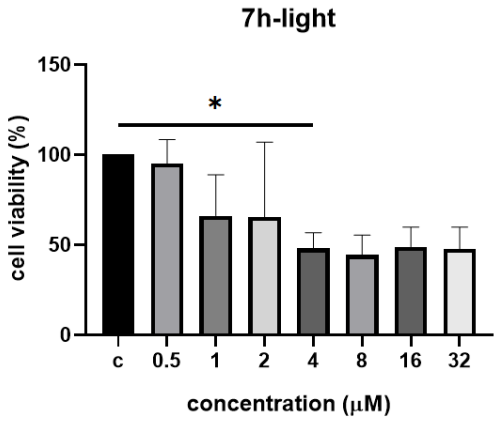

Figure 4.16. MCF-7 Cell viability assay results for molecule 7H in light group. n=3, * p<0.005

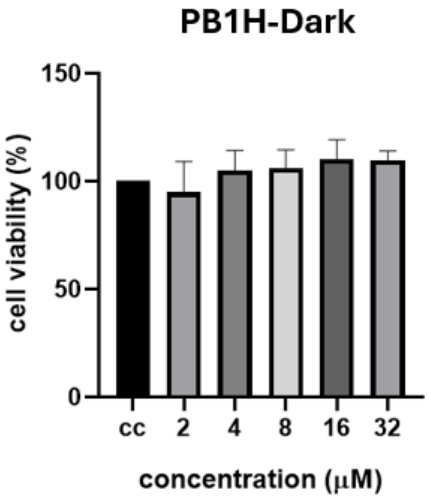

Figure 4.17. MCF-7 Cell viability assay results for molecule PB1H in dark group.

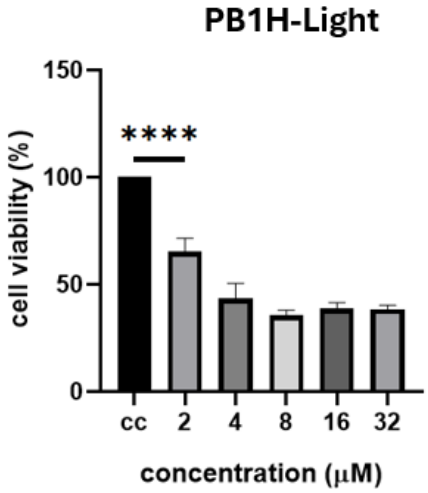

Figure 4.18. MCF-7 Cell viability assay results for molecule PB1H in light group. n=3, **** p<0.0001

Figure 4.19 shows the effect of molecule 7 on MCF-7 cell line in dark group. According to the result, molecule 7 does not show dark toxicity. Despite this result, in light group, a decrease was observed starting from the 0.25μM (Figure 4.20). The EC50 value for this molecule is estimated around 1 μM.

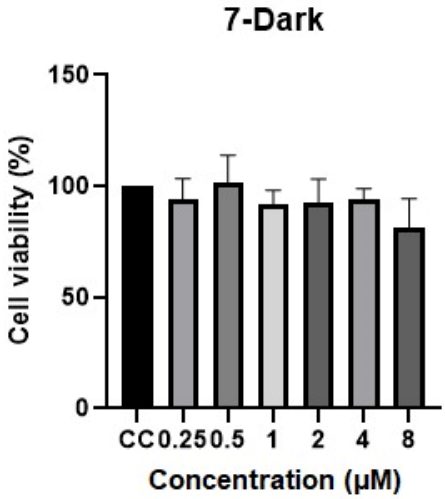

Figure 4.19. MCF-7 Cell viability assay results for molecule 7 in dark group.

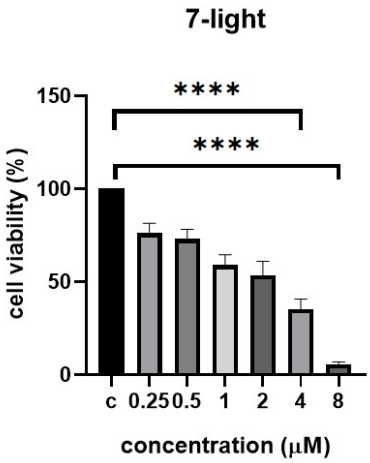

Figure 4.20. MCF-7 Cell viability assay results for molecule PB1H in light group. n=3, **** p<0.0001

MTT assay results of molecule PB1 indicates that PB1 has not showing dark toxicity towards MCF-7 cells in dark control (Figure 4.21), on the other hand in the light group, cell viability was affected by the designed PS (Figure 4.22). The EC50 for caged-PS PB1 is estimated around 8 μM. When, compared to PS 7, it has been shown that, there is decreased efficiency in ROS formation and photocytotoxicity when hydrazone bonds were employed. This shows that the caging effect is successful for 7/PB1 couple, which shows the potential of these structures to be employed in pH-controlled activation in cancer microenvironment.

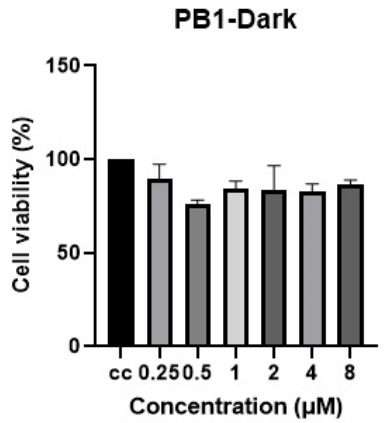

Figure 4.21. MCF-7 Cell viability assay results for molecule PB1 in dark group.

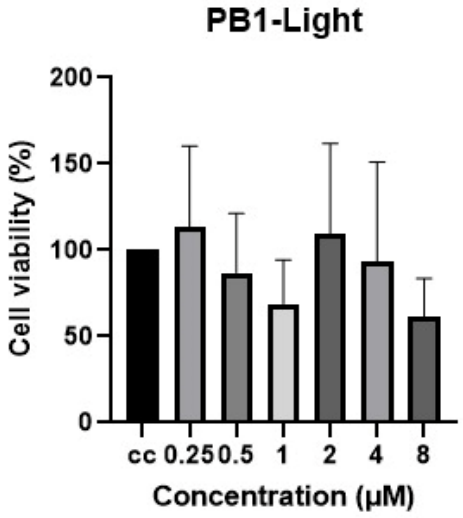

Figure 4.22. MCF-7 Cell viability assay results for molecule PB1 in light group.

5. CONCLUSIONS AND RECOMMENDATIONS

5.1. Conclusion

In this thesis, five novel BODIPY based near-IR absorbing, aqueous medium soluble, low pH activatable hydrazone-based PSs were designed and synthesized. The design strategy was based on the caged-photosensitizer prodrug (**PB1**) remaining intact in healthy cells, while in the acidic environment of cancerous tissues, the hydrazone unit hydrolyzes, converting into the activated aldehyde form (**7**) and thereby switching on the treatment mode. One of the key requirements of photodynamic therapy (PDT)—photosensitizer (PS) activation in the near-infrared (NIR) region—was successfully addressed in this study. Through structural modifications of BODIPY, the absorption peak was shifted from 500 nm (as seen in the parent BODIPY) to beyond 640 nm in our distyryl BODIPY molecules. To the best of our knowledge, this is the first report of distyryl-conjugated hydrazone-BODIPY structures. The synthesis of this family of molecules requires careful design considerations.

The initial steps of the study involved the design and synthesis of target molecules. However, during the Vilsmeier–Haack formylation reaction, an unexpected detachment of the iodine atom from the BODIPY core occurred in the major product. This led to the formation of halogen- and heavy atom-free derivatives—**7H**, **PB1H**, and **PB2H**. These molecules were also investigated and found to retain the ability to generate reactive oxygen species (ROS), as evidenced by the decrease in DPBF absorbance. Although halogen-free photosensitizers (PSs) typically exhibit lower ROS generation efficiency, cell viability assays still demonstrated their photodynamic efficacy. The significance of halogen-free PSs has also been highlighted in several previous studies (Cakmak et al. 2011). Minor products, including **7** and **PB1**, were also analyzed and exhibited respectable singlet oxygen quantum yields of 0.35 and 0.26, respectively. This finding suggests partial caging of the activated molecules *via* the hydrazone bond in the synthesized structures.

Following synthesis, hydrolysis studies revealed that the hydrazone-bearing molecule **PB1H** undergoes successful hydrolysis under mildly acidic conditions (DMSO: PBS, 4:1), gradually converting into the potentially active prodrug **7H**. In contrast, the dihydrazone molecule **PB2H** was found to hydrolyze even under neutral conditions, limiting its suitability for pH-triggered activation studies.

After the chemical ROS generation and hydrolysis experiments, the *in vitro* efficacy of the photosensitizers was evaluated using MCF-7 human breast cancer cells as

a model. The results aligned well with spectroscopic findings. The activated prodrug PS **7** exhibited high photocytotoxicity, with an EC_{50} value of approximately 2 μM. Meanwhile, the hydrazone-bearing, heavy-atom-free PS **PB1H** showed an EC_{50} of 8 μM. Its activated form, 7H, demonstrated enhanced activity with an EC_{50} of 4 μM, indicating improved efficacy upon activation.

These findings highlight the critical role of the hydrazone bond in maintaining the photosensitizer in an inactive state at neutral pH, while enabling activation under acidic conditions. Experimental results confirmed the hydrolysis mechanism, validating the pH-responsive activation strategy of the photosensitizer.

5.2. Recommendation

To further validate the activity of the synthesized prodrug photosensitizers, it would be beneficial to investigate the hydrolysis of the caged-hydrazone structures through in vitro studies using multiple cell lines.

6. REFERENCES

Abrahamse, Heidi, and Michael R. Hamblin. 2016. "New Photosensitizers for Photodynamic Therapy." *Biochemical Journal* 473(4): 347–64. doi:10.1042/BJ20150942.

Agazzi, Maximiliano L., M. Belén Ballatore, Andrés M. Durantini, Edgardo N. Durantini, and Augusto C. Tomé. 2019. "BODIPYs in Antitumoral and Antimicrobial Photodynamic Therapy: An Integrating Review." *Journal of Photochemistry and Photobiology C: Photochemistry Reviews* 40: 21–48. doi:10.1016/j.jphotochemrev.2019.04.001.

Agostinis, Patrizia, Kristian Berg, Keith A. Cengel, Thomas H. Foster, Albert W. Girotti, Sandra O. Gollnick, Stephen M. Hahn, et al. 2011. "Photodynamic Therapy of Cancer: An Update." *CA: A Cancer Journal for Clinicians* 61(4): 250–81. doi:10.3322/caac.20114.

Allison, Ron R., and Keyvan Moghissi. 2013. "Photodynamic Therapy (PDT): PDT Mechanisms." *Clinical Endoscopy* 46(1): 24–29. doi:10.5946/ce.2013.46.1.24.

Allison, Ron R., and Claudio H. Sibata. 2010. "Oncologic Photodynamic Therapy Photosensitizers: A Clinical Review." *Photodiagnosis and Photodynamic Therapy* 7(2): 61–75. doi:10.1016/j.pdpdt.2010.02.001.

Awuah, Samuel G., and Youngjae You. 2012. "Boron Dipyrromethene (BODIPY)-Based Photosensitizers for Photodynamic Therapy." *RSC Advances* 2(30): 11169–83. doi:10.1039/c2ra21404k.

Bonora, Massimo, Simone Patergnani, Alessandro Rimessi, Elena de Marchi, Jan M. Suski, Angela Bononi, Carlotta Giorgi, et al. 2012. "ATP Synthesis and Storage." *Purinergic Signalling* 8(3): 343–57. doi:10.1007/s11302-012-9305-8.

Brunner, Henri, and Nick Gruber. 2004. "Carboplatin-Containing Porphyrin-Platinum Complexes as Cytotoxic and Phototoxic Antitumor Agents." *Inorganica Chimica Acta* 357(15): 4423–51. doi:10.1016/j.ica.2004.03.061.

Cakmak, Yusuf, Safacan Kolemen, Selin Duman, Yavuz Dede, Yusuf Dolen, Bilal Kilic, Ziya Kostereli, et al. 2011. "Designing Excited States: Theory-Guided Access to Efficient Photosensitizers for Photodynamic Action." *Angewandte Chemie* 123(50): 12143–47. doi:10.1002/ange.201105736.

Calin, M. A., and S. V. Parasca. 2006. "Photodynamic Therapy in Oncology." In *Journal of Optoelectronics and Advanced Materials*, National Institute of Optoelectronics, 1173–79. doi:10.1634/theoncologist.11-9-1034.

Calzavara-Pinton, P. G., M. Venturini, and R. Sala. 2005. "A Comprehensive Overview of Photodynamic Therapy in the Treatment of Superficial Fungal Infections of the Skin." *Journal of Photochemistry and Photobiology B: Biology* 78(1): 1–6. doi:10.1016/j.jphotobiol.2004.06.006.

Castano, Ana P., Tatiana N. Demidova, and Michael R. Hamblin. 2005. “Mechanisms in Photodynamic Therapy: Part Two - Cellular Signaling, Cell Metabolism and Modes of Cell Death.” *Photodiagnosis and Photodynamic Therapy* 2(1 SPEC. ISS.): 1–23. doi:10.1016/S1572-1000(05)00030-X.

Correia, José H., José A. Rodrigues, Sara Pimenta, Tao Dong, and Zhaochu Yang. 2021. “Photodynamic Therapy Review: Principles, Photosensitizers, Applications, and Future Directions.” *Pharmaceutics* 13(9). doi:10.3390/pharmaceutics13091332.

Fernandez, Antonio, Matthieu Vermeren, Duncan Humphries, Ramon Subiros-Funosas, Nicole Barth, Lara Campana, Alison Mackinnon, Yi Feng, and Marc Vendrell. 2017. “Chemical Modulation of in Vivo Macrophage Function with Subpopulation-Specific Fluorescent Prodrug Conjugates.” *ACS Central Science* 3(9): 995–1005. doi:10.1021/acscentsci.7b00262.

Fink, Susan L., and Brad T. Cookson. 2005. “Apoptosis, Pyroptosis, and Necrosis: Mechanistic Description of Dead and Dying Eukaryotic Cells.” *Infection and Immunity* 73(4): 1907–16. doi:10.1128/IAI.73.4.1907-1916.2005.

Gunaydin, Gurcan, M. Emre Gedik, and Seylan Ayan. 2021. “Photodynamic Therapy for the Treatment and Diagnosis of Cancer–A Review of the Current Clinical Status.” *Frontiers in Chemistry* 9. doi:10.3389/fchem.2021.686303.

Hamblin, Michael R. 2020. “Photodynamic Therapy for Cancer: What’s Past Is Prologue.” *Photochemistry and Photobiology* 96(3): 506–16. doi:10.1111/php.13190.

Hu, Zhiwei. 2014. “Photodynamic Therapy as an Emerging Treatment Modality for Cancer and Non-Cancer Diseases.” *Journal of Analytical & Bioanalytical Techniques* S1(e001). doi:10.4172/2155-9872.s1-e001.

Kang, Hyunkoo, Byeongsoo Kim, Junhyeong Park, Hye Sook Youn, and Bu Hyun Youn. 2023. “The Warburg Effect on Radioresistance: Survival beyond Growth.” *Biochimica et Biophysica Acta - Reviews on Cancer* 1878(6). doi:10.1016/j.bbcan.2023.188988.

Kowada, Toshiyuki, Hiroki Maeda, and Kazuya Kikuchi. 2015. “BODIPY-Based Probes for the Fluorescence Imaging of Biomolecules in Living Cells.” *Chemical Society Reviews* 44(14): 4953–72. doi:10.1039/c5cs00030k.

Krimalowski, Alexander, and Mukundan Thelakkat. 2019. “Sequential Co-Click Reactions with Poly(Glycidyl Propargyl Ether) toward Single-Ion Conducting Electrolytes.” *Macromolecules* 52(11): 4042–51. doi:10.1021/acs.macromol.9b00206.

Lan, Minhuan, Shaojing Zhao, Weimin Liu, Chun Sing Lee, Wenjun Zhang, and Pengfei Wang. 2019. “Photosensitizers for Photodynamic Therapy.” *Advanced Healthcare Materials* 8(13). doi:10.1002/adhm.201900132.

Li, Wen, Jingtian Zhang, Zhiyuan Gao, Ji Qi, and Dan Ding. 2022. “Advancing Biomedical Applications via Manipulating Intersystem Crossing.” *Coordination Chemistry Reviews* 471. doi:10.1016/j.ccr.2022.214754.

Li, Xingshu, Safacan Kolemen, Juyoung Yoon, and Engin U. Akkaya. 2017. “Activatable Photosensitizers: Agents for Selective Photodynamic Therapy.” *Advanced Functional Materials* 27(5). doi:10.1002/adfm.201604053.

Li, Zhiheng, Zhenwu Zhou, Yarui Wang, Jie Wang, Liming Zhou, Hong Bo Cheng, and Juyoung Yoon. 2023. “Activatable Nano-Photosensitizers for Precise Photodynamic Cancer Therapy.” *Coordination Chemistry Reviews* 493. doi:10.1016/j.ccr.2023.215324.

Liao, Senyi, Guang Wu, Zhizhong Xie, Xiaoyong Lei, Xiaoyan Yang, Sheng Huang, Xiangping Deng, Zhe Wang, and Guotao Tang. 2024. “PH Regulators and Their Inhibitors in Tumor Microenvironment.” *European Journal of Medicinal Chemistry* 267. doi:10.1016/j.ejmech.2024.116170.

Lin, Baoping, Heting Chen, Danyang Liang, Wei Lin, Xiaoyang Qi, Hanping Liu, and Xiaoyuan Deng. 2019. “Acidic PH and High-H 2 O 2 Dual Tumor Microenvironment-Responsive Nanocatalytic Graphene Oxide for Cancer Selective Therapy and Recognition.” *ACS Applied Materials and Interfaces* 11(12): 11157–66. doi:10.1021/acsami.8b22487.

Lovell, Jonathan F., Tracy W.B. Liu, Juan Chen, and Gang Zheng. 2010. “Activatable Photosensitizers for Imaging and Therapy.” *Chemical Reviews* 110(5): 2839–57. doi:10.1021/cr900236h.

Mattila, Heta, Sergey Khorobrykh, Vesa Havurinne, and Esa Tyystjärvi. 2015. “Reactive Oxygen Species: Reactions and Detection from Photosynthetic Tissues.” *Journal of Photochemistry and Photobiology B: Biology* 152: 176–214. doi:10.1016/j.jphotobiol.2015.10.001.

Mfouo-Tynga, Ivan S., Lucas D. Dias, Natalia M. Inada, and Cristina Kurachi. 2021a. “Features of Third Generation Photosensitizers Used in Anticancer Photodynamic Therapy: Review.” *Photodiagnosis and Photodynamic Therapy* 34. doi:10.1016/j.pdpdt.2020.102091.

Mfouo-Tynga, Ivan S., Lucas D. Dias, Natalia M. Inada, and Cristina Kurachi. 2021b. “Features of Third Generation Photosensitizers Used in Anticancer Photodynamic Therapy: Review.” *Photodiagnosis and Photodynamic Therapy* 34. doi:10.1016/j.pdpdt.2020.102091.

Mfouo-Tynga, Ivan S., Lucas D. Dias, Natalia M. Inada, and Cristina Kurachi. 2021c. “Features of Third Generation Photosensitizers Used in Anticancer Photodynamic Therapy: Review.” *Photodiagnosis and Photodynamic Therapy* 34. doi:10.1016/j.pdpdt.2020.102091.

Mitton, D., and R. Ackroyd. 2005. “History of Photodynamic Therapy in Great Britain.” *Photodiagnosis and Photodynamic Therapy* 2(4): 239–46. doi:10.1016/S1572-1000(05)00111-0.

Nestoros, Eleni, Amit Sharma, Eunji Kim, Jong Seung Kim, and Marc Vendrell. 2024. "Smart Molecular Designs and Applications of Activatable Organic Photosensitizers." *Nature Reviews Chemistry*. doi:10.1038/s41570-024-00662-7.

Olszowy, Marta, Martyna Nowak-Perlak, and Marta Woźniak. 2023. "Current Strategies in Photodynamic Therapy (PDT) and Photodynamic Diagnostics (PDD) and the Future Potential of Nanotechnology in Cancer Treatment." *Pharmaceutics* 15(6). doi:10.3390/pharmaceutics15061712.

Ozdemir, Mehmet, Donghee Choi, Guhyun Kwon, Yunus Zorlu, Bunyemin Cosut, Hye-Kyung Kim, Antonio Facchetti, Choongik Kim, and Hakan Usta. 2022. *Solution-Processable BODIPY-Based Small Molecules for Semiconducting Microfibers in Organic Thin-Film Transistors*.

Radunz, Sebastian, Stefanie Wedepohl, Mathilde Röhr, Marcelo Calderón, Harald Rune Tschiche, and Ute Resch-Genger. 2020. "PH-Activatable Singlet Oxygen-Generating Boron-Dipyrromethenes (BODIPYs) for Photodynamic Therapy and Bioimaging." *Journal of Medicinal Chemistry* 63(4): 1699–1708. doi:10.1021/acs.jmedchem.9b01873.

Robertson, C. A., D. Hawkins Evans, and H. Abrahamse. 2009. "Photodynamic Therapy (PDT): A Short Review on Cellular Mechanisms and Cancer Research Applications for PDT." *Journal of Photochemistry and Photobiology B: Biology* 96(1): 1–8. doi:10.1016/j.jphotobiol.2009.04.001.

Rowan, Stuart J., Stuart J. Cantrill, Graham R.L. Cousins, Jeremy K.M. Sanders, and J. Fraser Stoddart. 2002. "Dynamic Covalent Chemistry." *Angewandte Chemie - International Edition* 41(6): 898–952. doi:10.1002/1521-3773(20020315)41:6<898::aid-anie898>3.0.co;2-e.

Rybczynski, Patryk, Aleksander Smolarkiewicz-Wyczachowski, Jaroslaw Piskorz, Szymon Bocian, Marta Ziegler-Borowska, Dariusz Kędziera, and Anna Kaczmarek-Kędziera. 2021. "Photochemical Properties and Stability of Bodipy Dyes." *International Journal of Molecular Sciences* 22(13). doi:10.3390/ijms22136735.

Say, Büşra, Beytullah Tatar, Betül Üzülmez, Melike Ebrar Bakırcı, Gülcihan Gülseren, and Yusuf Cakmak. 2023. "Caging of Bodipy Photosensitizers through Hydrazone Bond Formation and Their Activation Dynamics." *ChemMedChem* 18(13). doi:10.1002/cmdc.202300199.

Schad, Christopher, Cesar Ray, Carolina Díaz-Norambuena, Sergio Serrano-Buitrago, Florencio Moreno, Beatriz L. Maroto, Inmaculada García-Moreno, et al. 2025. "Water-Soluble BODIPY Dyes: A Novel Approach for Their Sustainable Chemistry and Applied Photonics." *Chemical Science*. doi:10.1039/D5SC01295C.

Schweizer, Thorsten, Heiko Kubach, and Thomas Koch. 2021. "Investigations to Characterize the Interactions of Light Radiation, Engine Operating Media and Fluorescence Tracers for the Use of Qualitative Light-Induced Fluorescence in Engine Systems." *Automotive and Engine Technology* 6(3–4): 275–87. doi:10.1007/s41104-021-00092-3.

Singh, Praveen P., Surabhi Sinha, Prashant Gahtori, D. N. Mishra, Geetika Pandey, and Vishal Srivastava. 2024. "Recent Advancement in Photosensitizers for Photodynamic Therapy." *Dyes and Pigments* 229. doi:10.1016/j.dyepig.2024.112262.

Sonawane, Sandeep J., Rahul S. Kalhapure, and Thirumala Govender. 2017. "Hydrazone Linkages in PH Responsive Drug Delivery Systems." *European Journal of Pharmaceutical Sciences* 99: 45–65. doi:10.1016/j.ejps.2016.12.011.

Squeo, Benedetta M., Vasilis G. Gregoriou, Apostolos Avgeropoulos, Sebnem Baysec, Sybille Allard, Ullrich Scherf, and Christos L. Chochos. 2017. "BODIPY-Based Polymeric Dyes as Emerging Horizon Materials for Biological Sensing and Organic Electronic Applications." *Progress in Polymer Science* 71: 26–52. doi:10.1016/j.progpolymsci.2017.02.003.

Tatar, Beytullah, Büşra Say, Zeynep Demirsoy, Ayşe İlayda Boyacı, Gülcihan Gülseren, and Yusuf Cakmak. 2025. "Design and Synthesis of Hydrazone-Substituted BODIPY Derivatives for Photodynamic Therapy." *Journal of Photochemistry and Photobiology A: Chemistry* 469. doi:10.1016/j.jphotochem.2025.116592.

Tatum, Luke A., Xin Su, and Ivan Aprahamian. 2014. "Simple Hydrazone Building Blocks for Complicated Functional Materials." *Accounts of Chemical Research* 47(7): 2141–49. doi:10.1021/ar500111f.

Tavakkoli Yaraki, Mohammad, Bin Liu, and Yen Nee Tan. 2022. "Emerging Strategies in Enhancing Singlet Oxygen Generation of Nano-Photosensitizers Toward Advanced Phototherapy." *Nano-Micro Letters* 14(1). doi:10.1007/s40820-022-00856-y.

Turan, Ilke Simsek, Fatma Pir Cakmak, Deniz Cansen Yildirim, Rengul Cetin-Atalay, and Engin U. Akkaya. 2014. "Near-IR Absorbing BODIPY Derivatives as Glutathione-Activated Photosensitizers for Selective Photodynamic Action." *Chemistry - A European Journal* 20(49): 16088–92. doi:10.1002/chem.201405450.

Turksoy, Abdurrahman, Deniz Yildiz, and Engin U. Akkaya. 2019. "Photosensitization and Controlled Photosensitization with BODIPY Dyes." *Coordination Chemistry Reviews* 379: 47–64. doi:10.1016/j.ccr.2017.09.029.

Wang, Danfeng, Xin Wang, Shiyuan Zhou, Peiyang Gu, Xiaolin Zhu, Chengyuan Wang, and Qichun Zhang. 2023. "Evolution of BODIPY as Triplet Photosensitizers from Homogeneous to Heterogeneous: The Strategies of Functionalization to Various Forms and Their Recent Applications." *Coordination Chemistry Reviews* 482. doi:10.1016/j.ccr.2023.215074.

Wei, Min, Xin He, Na Liu, and Hui Deng. 2024. "Role of Reactive Oxygen Species in Ultraviolet-Induced Photodamage of the Skin." *Cell Division* 19(1). doi:10.1186/s13008-024-00107-z.

Yogo, Takatoshi, Yasuteru Urano, Yukiko Ishitsuka, Fumio Maniwa, and Tetsuo Nagano. 2005. "Highly Efficient and Photostable Photosensitizer Based on BODIPY

Chromophore." *Journal of the American Chemical Society* 127(35): 12162–63. doi:10.1021/ja0528533.

Yoshida, Takayuki, Tsz Chung Lai, Glen S. Kwon, and Kazuhiro Sako. 2013. "PH-and Ion-Sensitive Polymers for Drug Delivery." *Expert Opinion on Drug Delivery* 10(11): 1497–1513. doi:10.1517/17425247.2013.821978.

Yu, Xiao Tong, Shang Yan Sui, Yu Xuan He, Chen Hao Yu, and Qiang Peng. 2022. "Nanomaterials-Based Photosensitizers and Delivery Systems for Photodynamic Cancer Therapy." *Biomaterials Advances* 135. doi:10.1016/j.bioadv.2022.212725.

Zafar, Aasma, Summaiya Khatoon, Muhammad Jawad Khan, Junaid Abu, and Aisha Naeem. 2025. "Advancements and Limitations in Traditional Anti-Cancer Therapies: A Comprehensive Review of Surgery, Chemotherapy, Radiation Therapy, and Hormonal Therapy." *Discover Oncology* 16(1). doi:10.1007/s12672-025-02198-8.

Zane, C., E. Facchinetti, M. T. Rossi, C. Specchia, and P. G. Calzavara-Pinton. 2014. "A Randomized Clinical Trial of Photodynamic Therapy with Methyl Aminolaevulinate vs. Diclofenac 3% plus Hyaluronic Acid Gel for the Treatment of Multiple Actinic Keratoses of the Face and Scalp." *British Journal of Dermatology* 170(5): 1143–50. doi:10.1111/bjd.12844.

Zhang, Juan, Chengshi Jiang, João Paulo Figueiró Longo, Ricardo Bentes Azevedo, Hua Zhang, and Luis Alexandre Muehlmann. 2018. "An Updated Overview on the Development of New Photosensitizers for Anticancer Photodynamic Therapy." *Acta Pharmaceutica Sinica B* 8(2): 137–46. doi:10.1016/j.apsb.2017.09.003.

APPENDIX

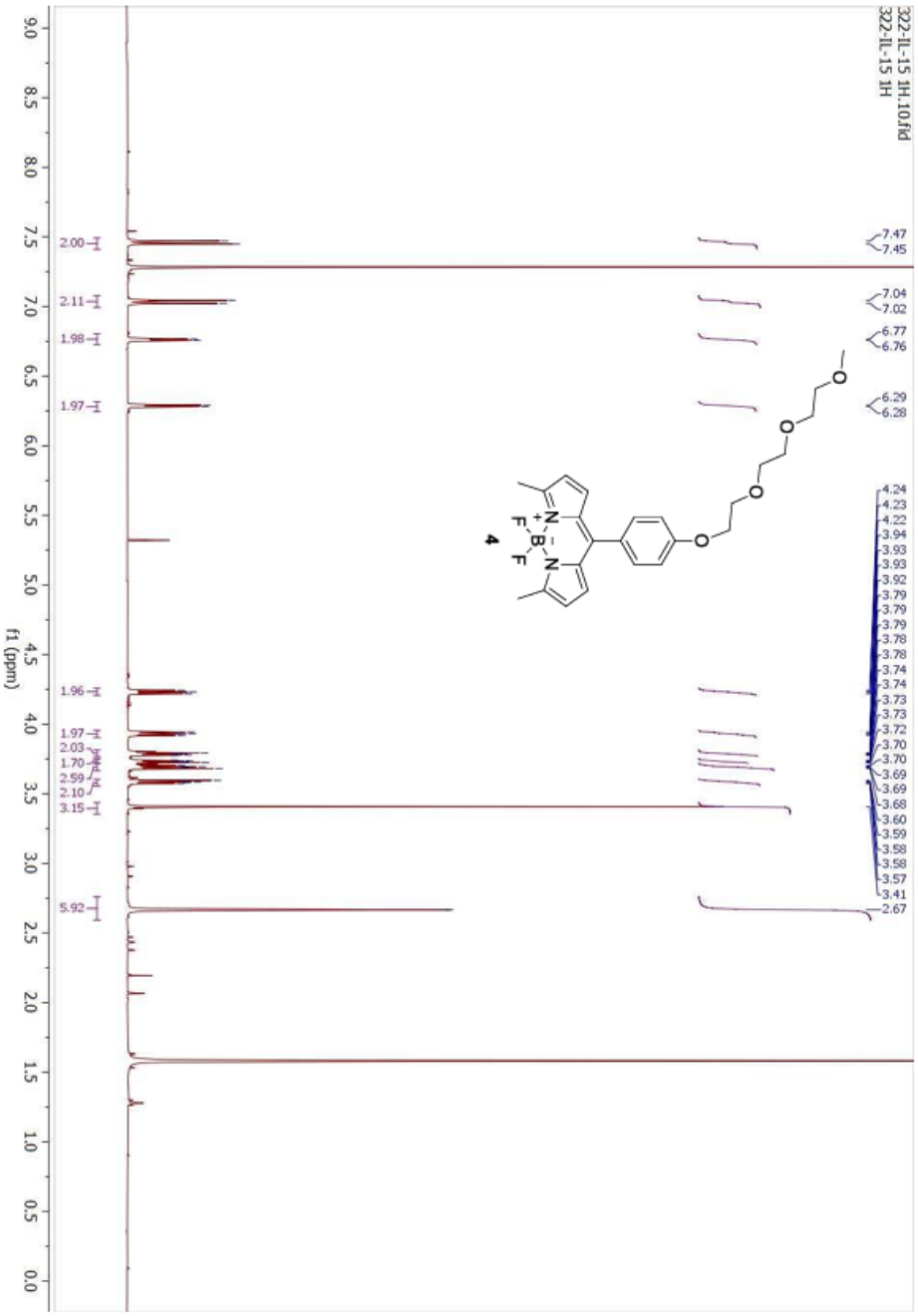

APPENDIX--1. ^{1}H NMR spectrum of molecule 4 ($CDCl_3$, 400 MHz)

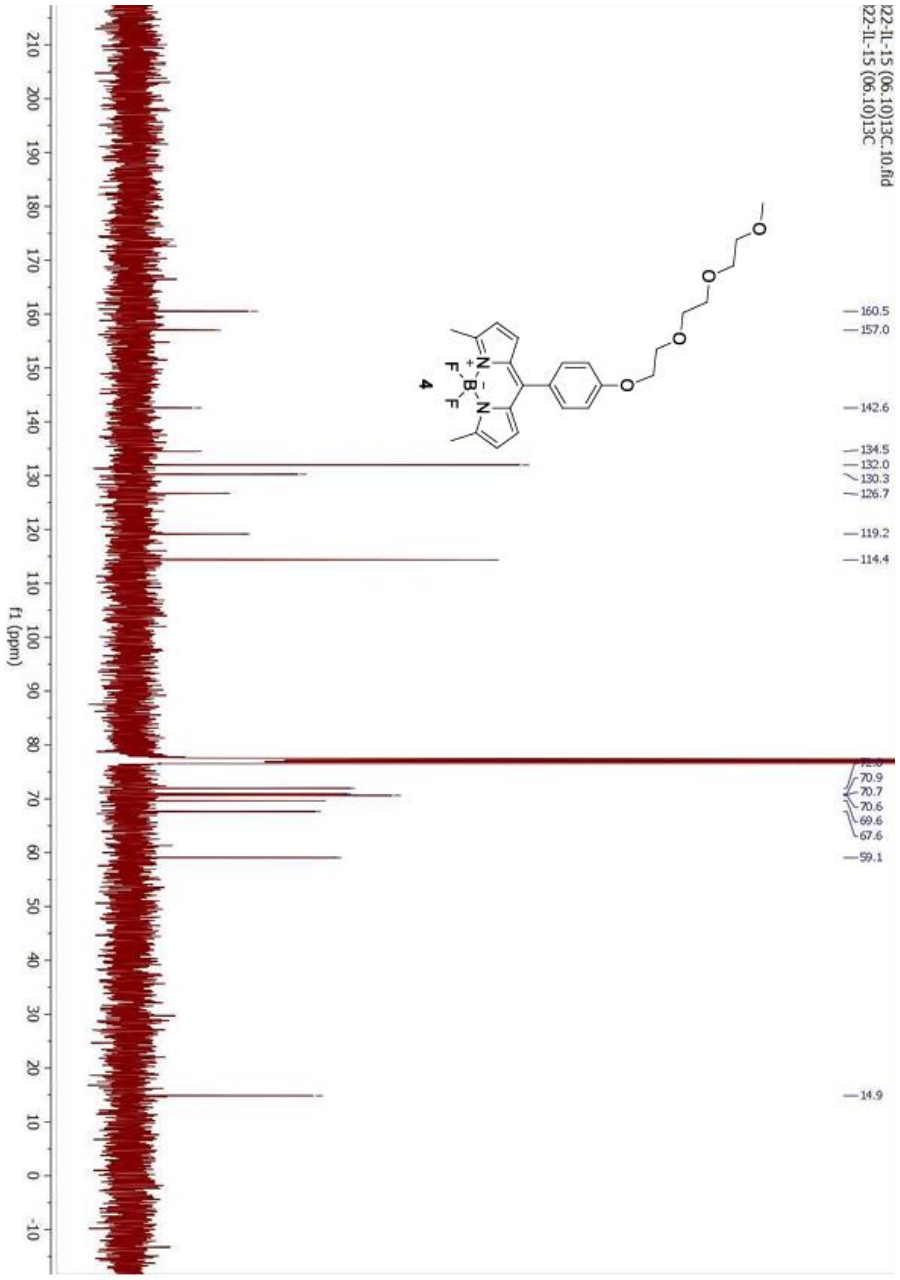

APPENDIX--2. ^{13}C NMR spectrum of molecule 4 ($CDCl_3$, 400 MHz)

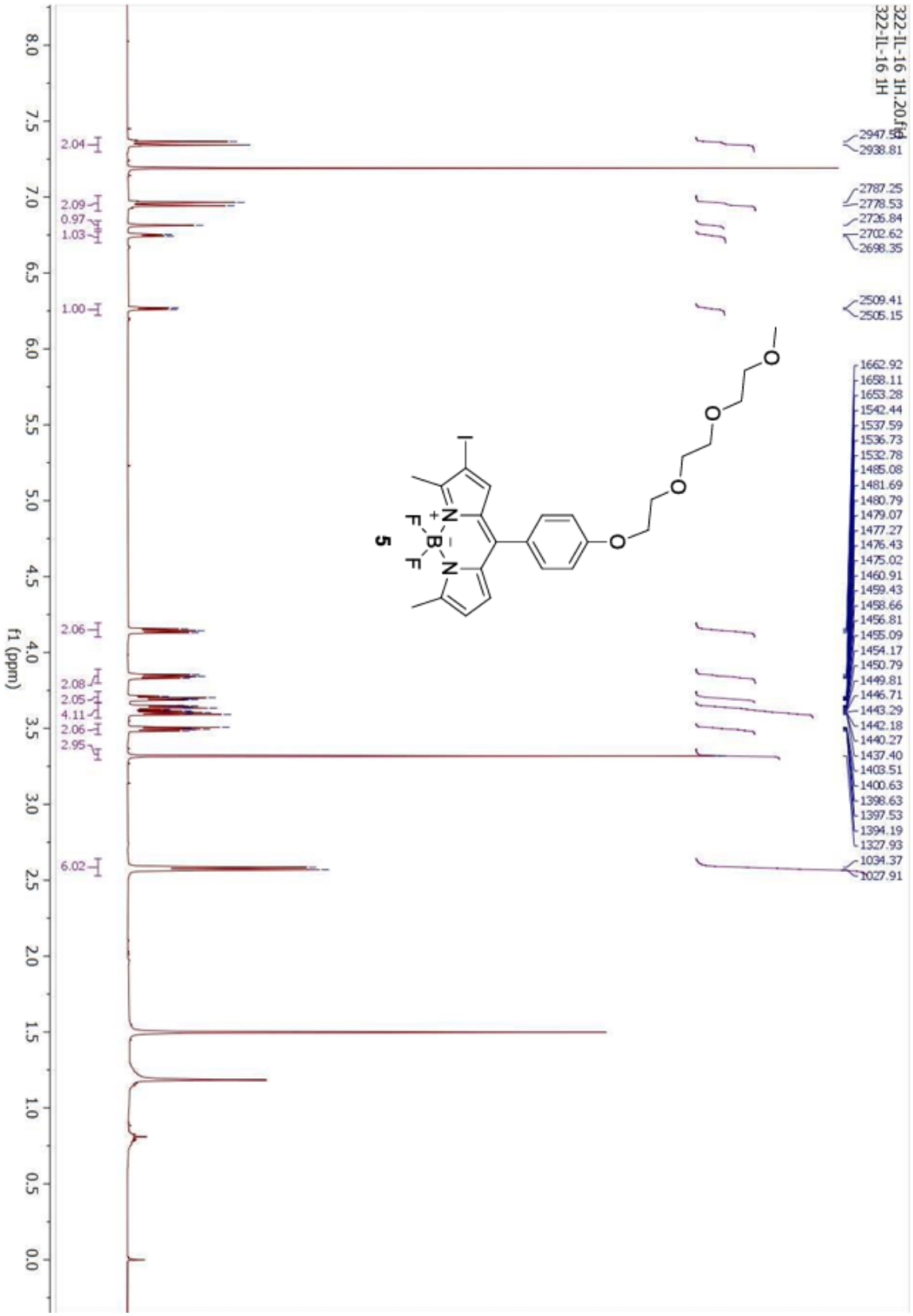

APPENDIX- 3. ^{1}H NMR spectrum of molecule 5 ($CDCl_3$, 400 MHz)

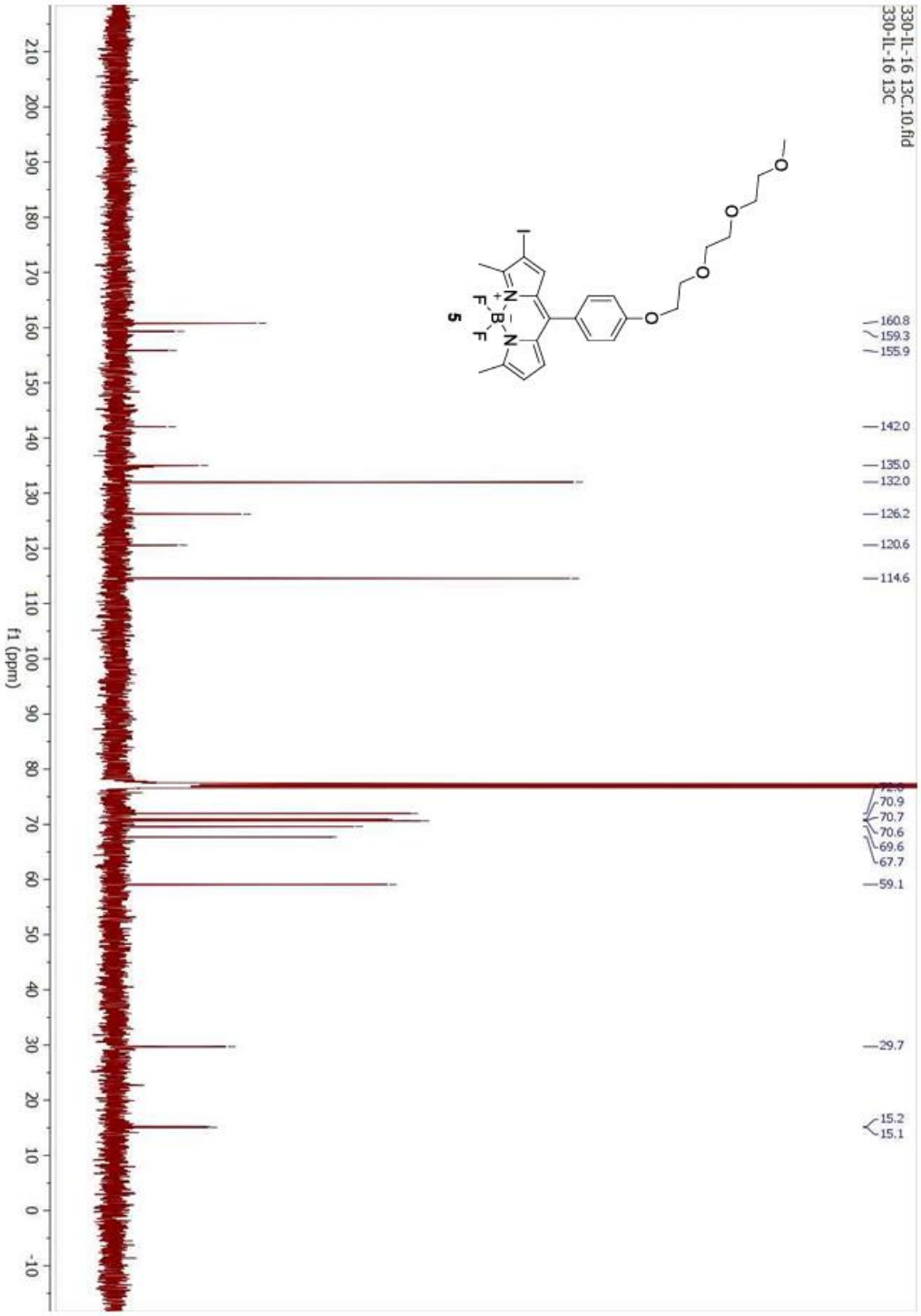

APPENDIX- 4. ^{13}C NMR spectrum of molecule 5 ($CDCl_3$, 400 MHz)

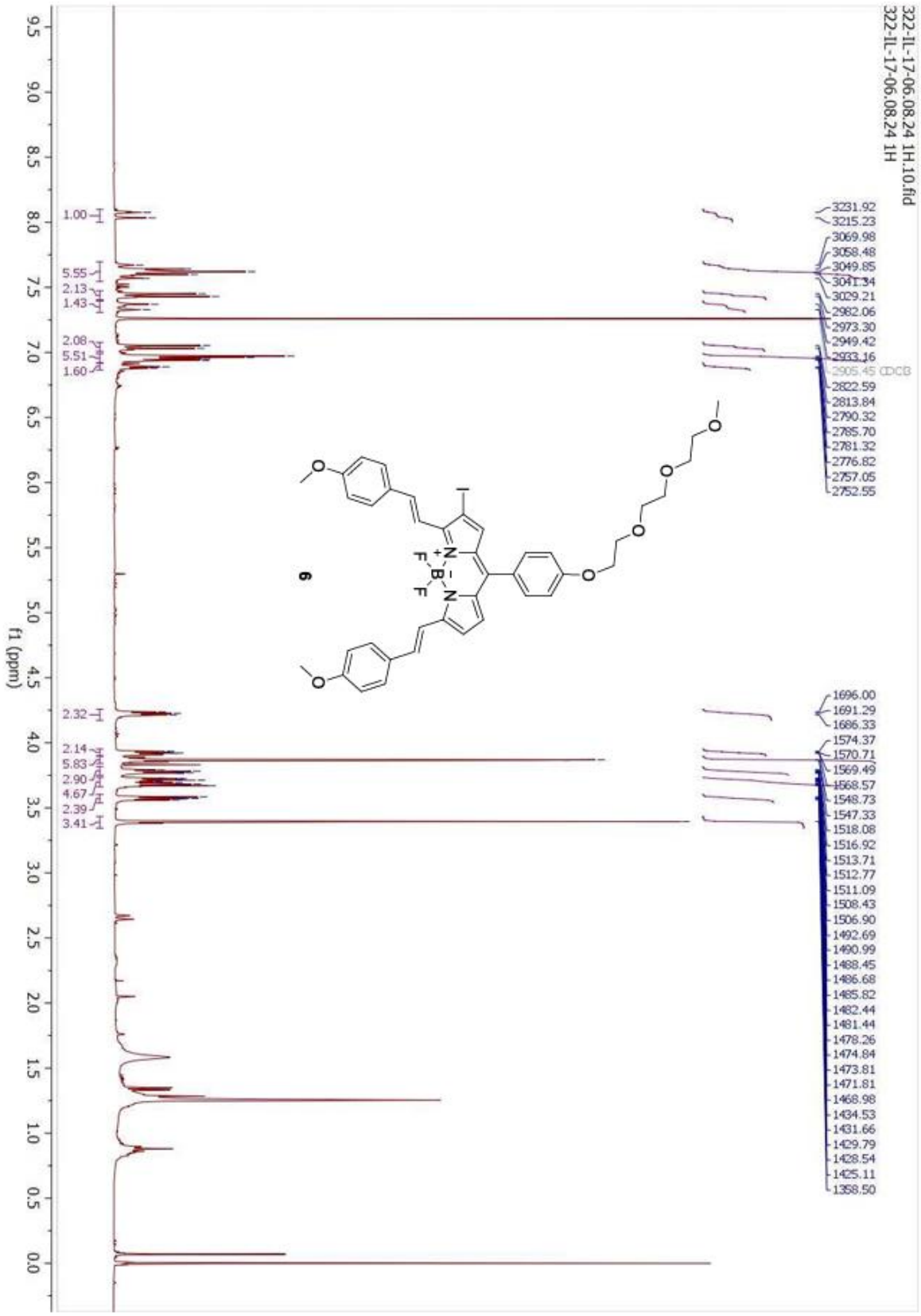

APPENDIX-5. ^{1}H NMR spectrum of molecule 6 ($CDCl_3$, 400 MHz)

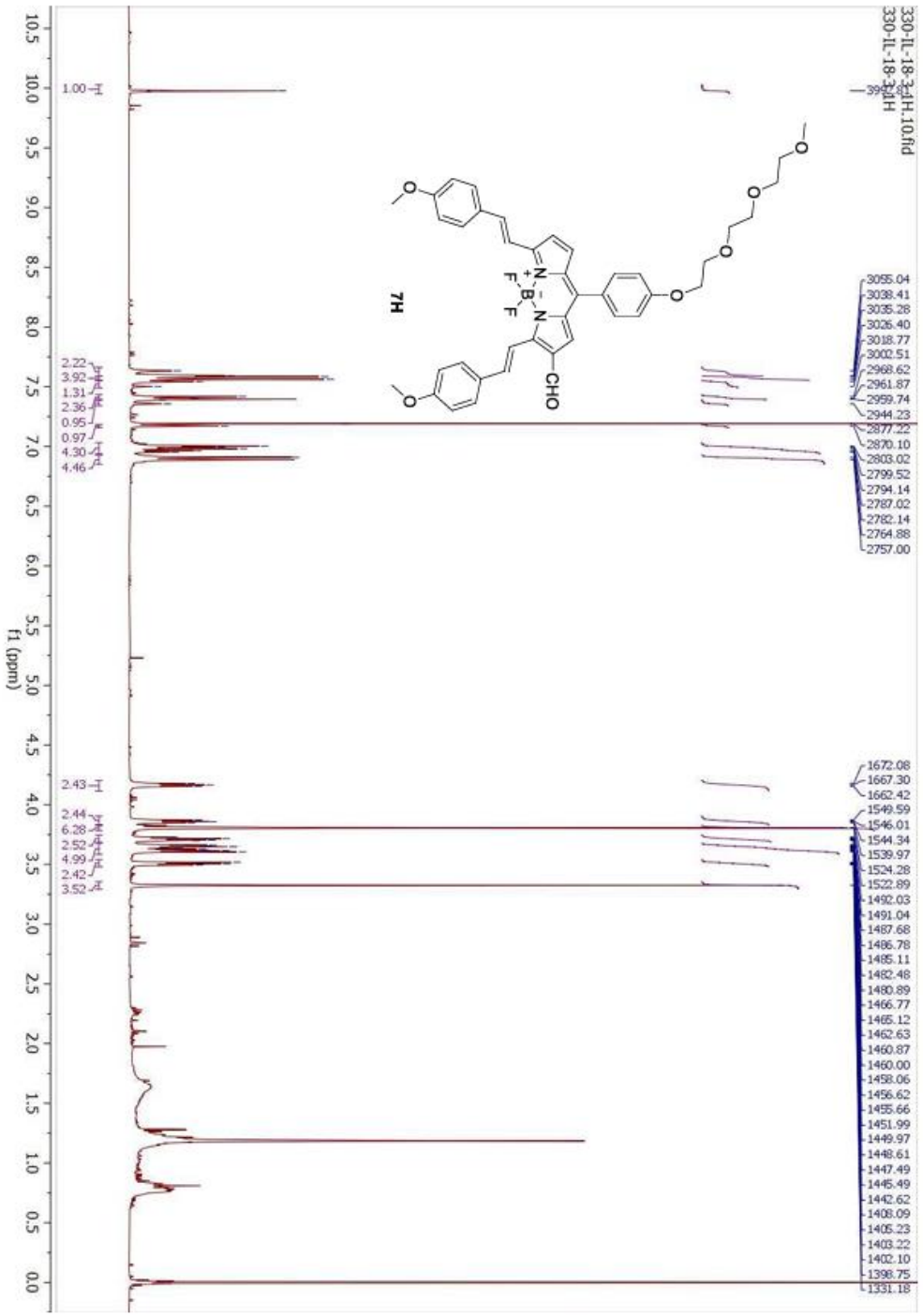

APPENDIX-6. ^{1}H NMR spectrum of molecule 7H ($CDCl_3$, 400 MHz)

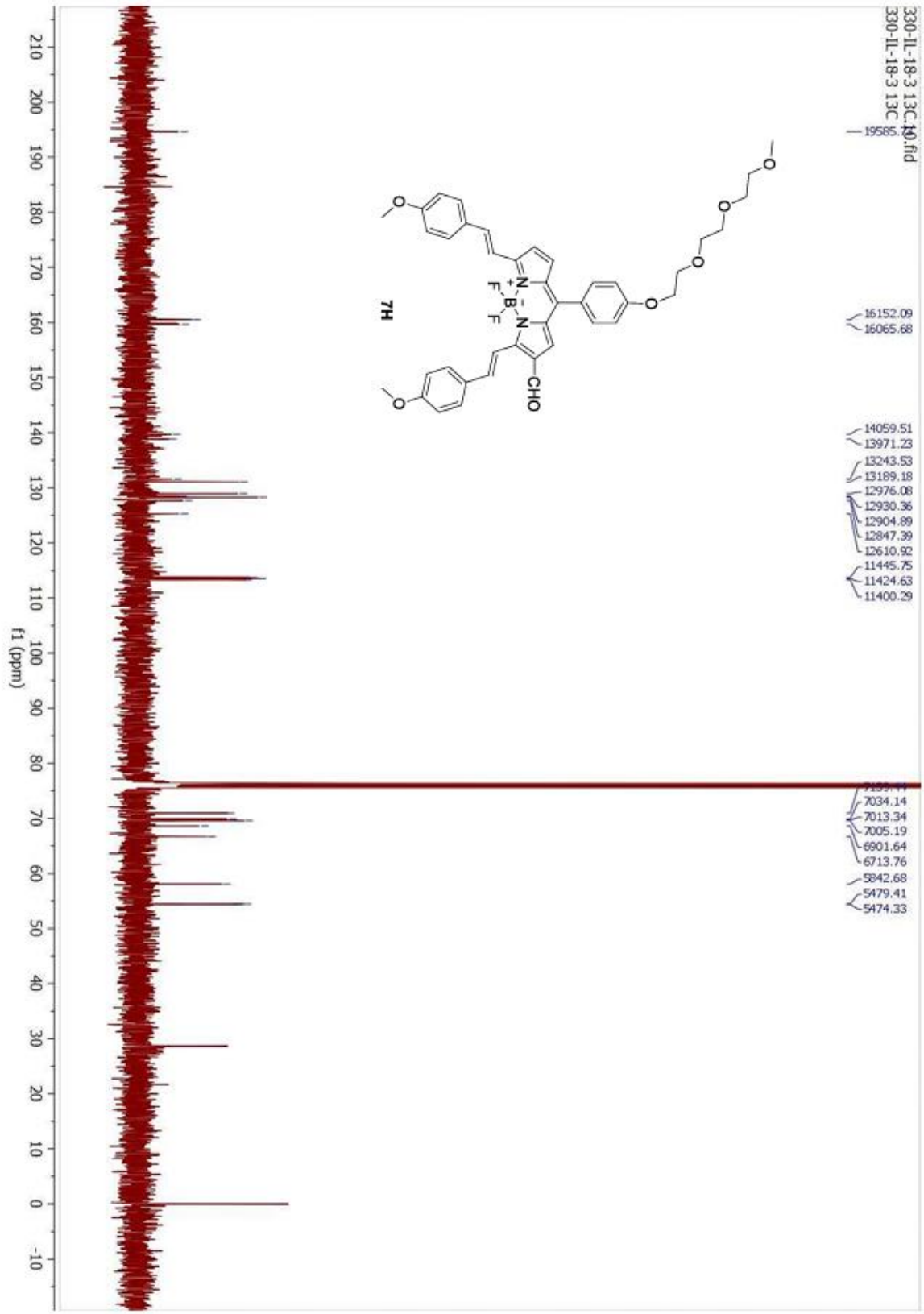

APPENDIX-7. ^{13}C NMR spectrum of molecule 7H ($CDCl_3$, 400 MHz)

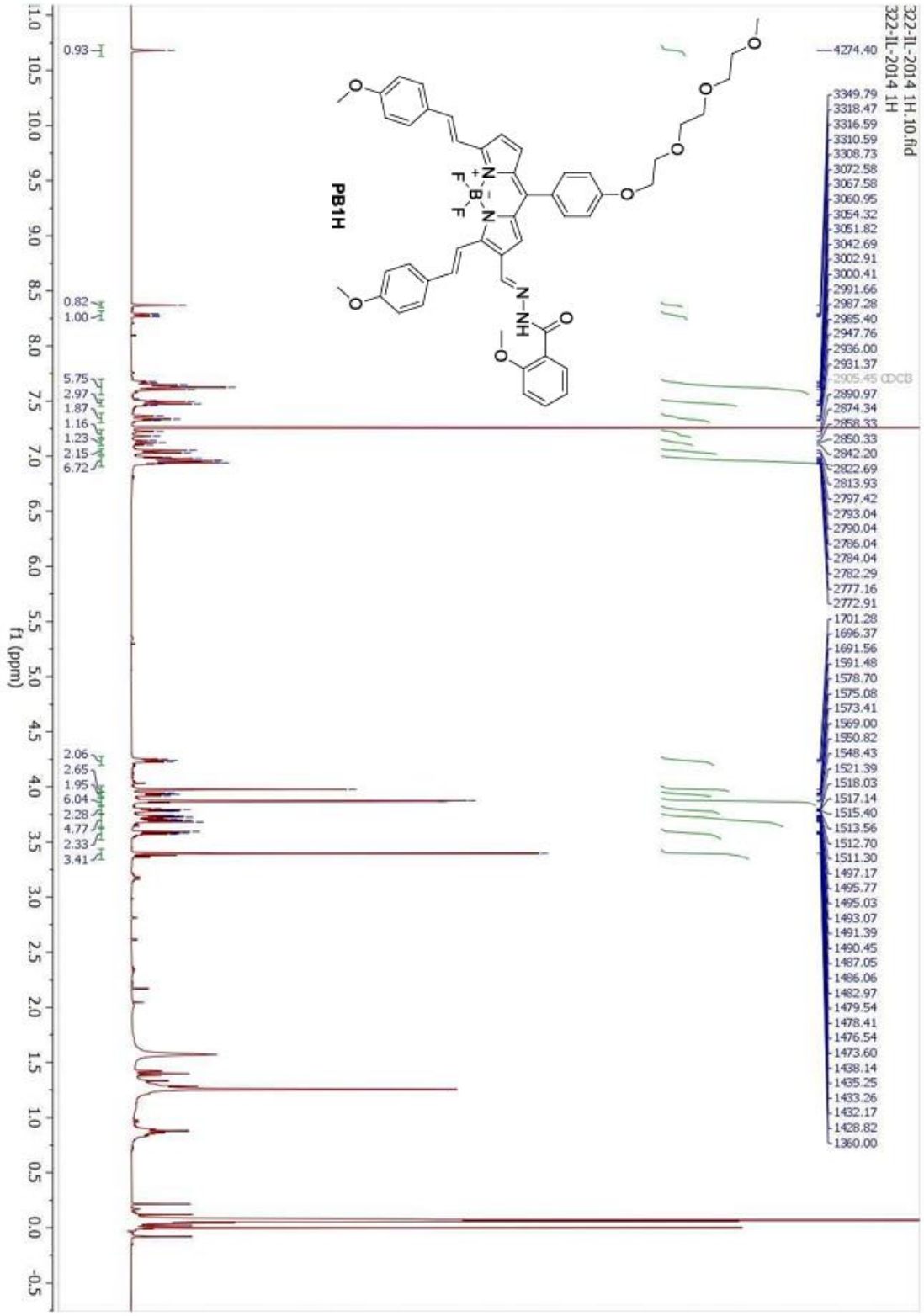

APPENDIX-8. ^{1}H NMR spectrum of molecule PB1H ($CDCl_3$, 400 MHz)

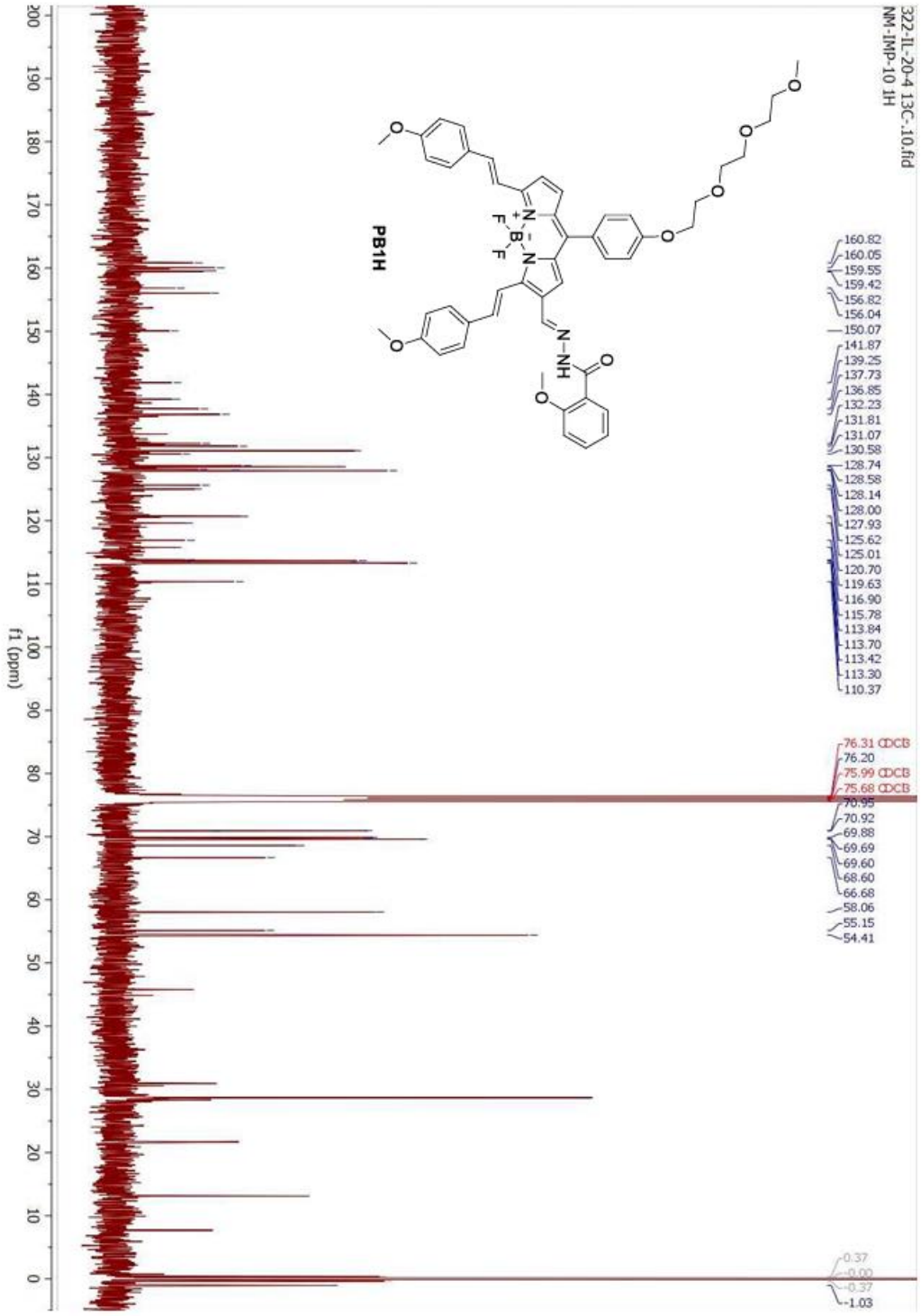

APPENDIX-9. ^{13}C NMR spectrum of molecule PB1H ($CDCl_3$, 400 MHz)

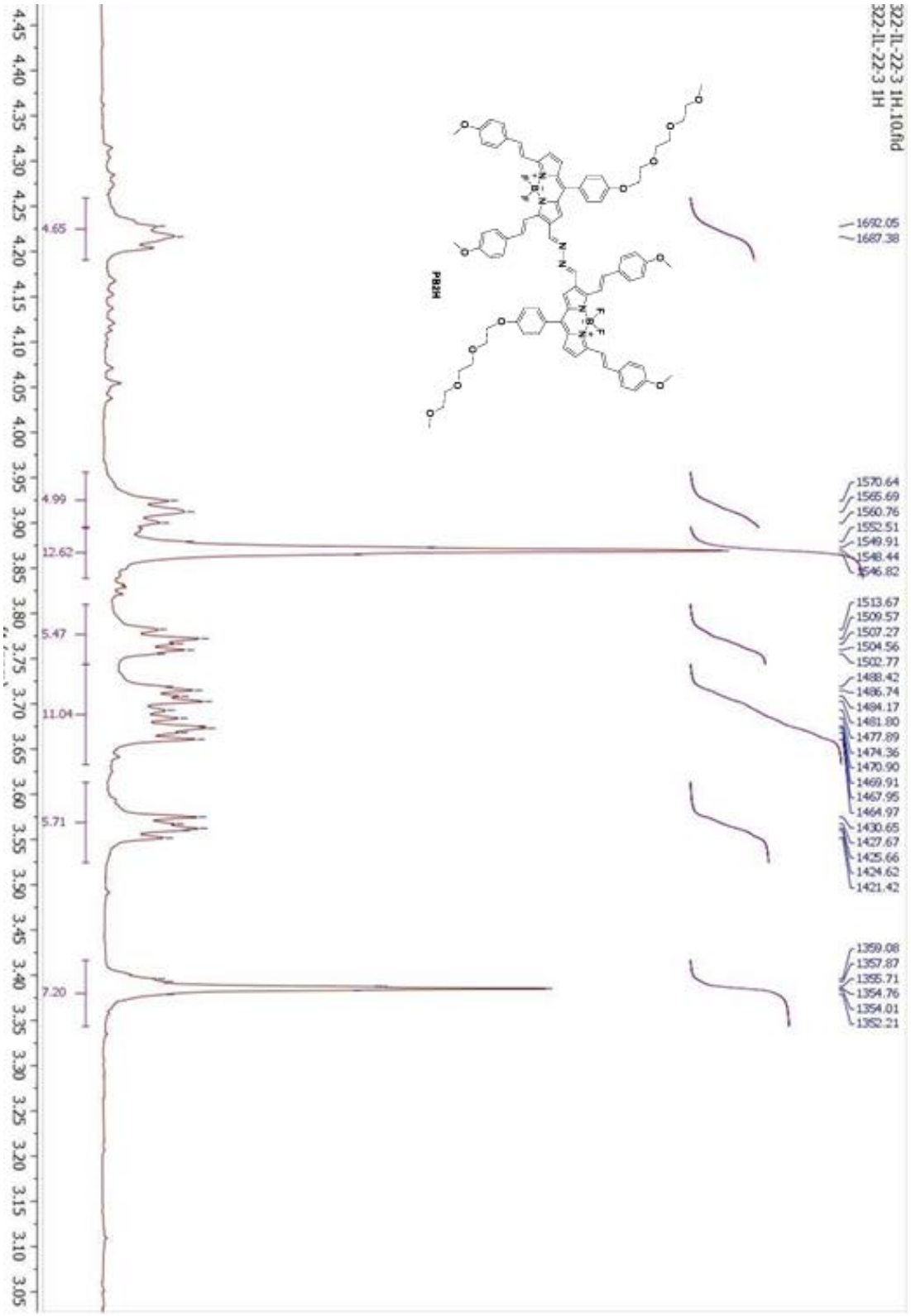

APPENDIX-10. ^{1}H NMR spectrum of molecule PB2H ($CDCl_3$, 400 MHz)

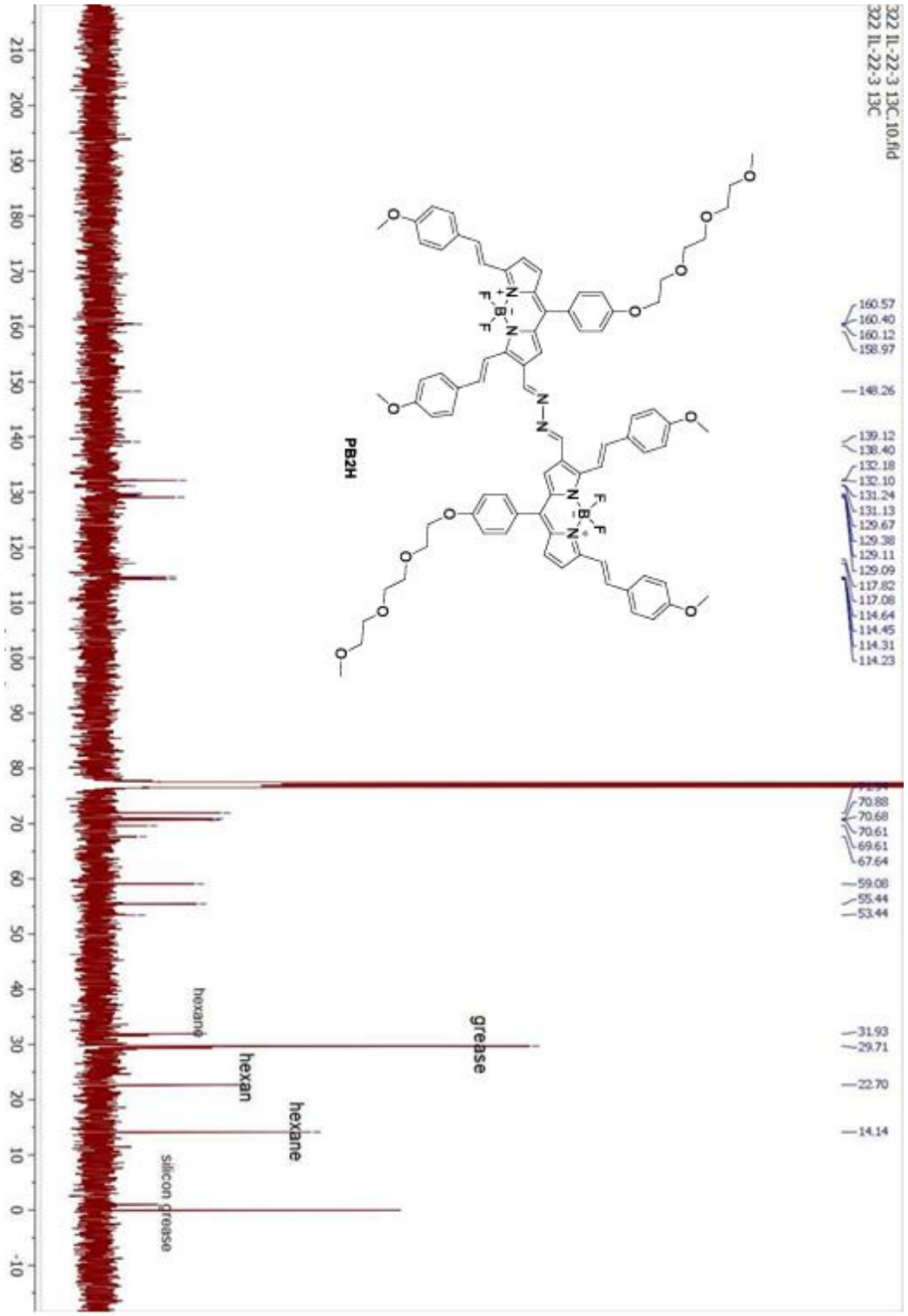

APPENDIX-11. ^{13}C NMR spectrum of molecule PB2H ($CDCl_3$, 400 MHz)

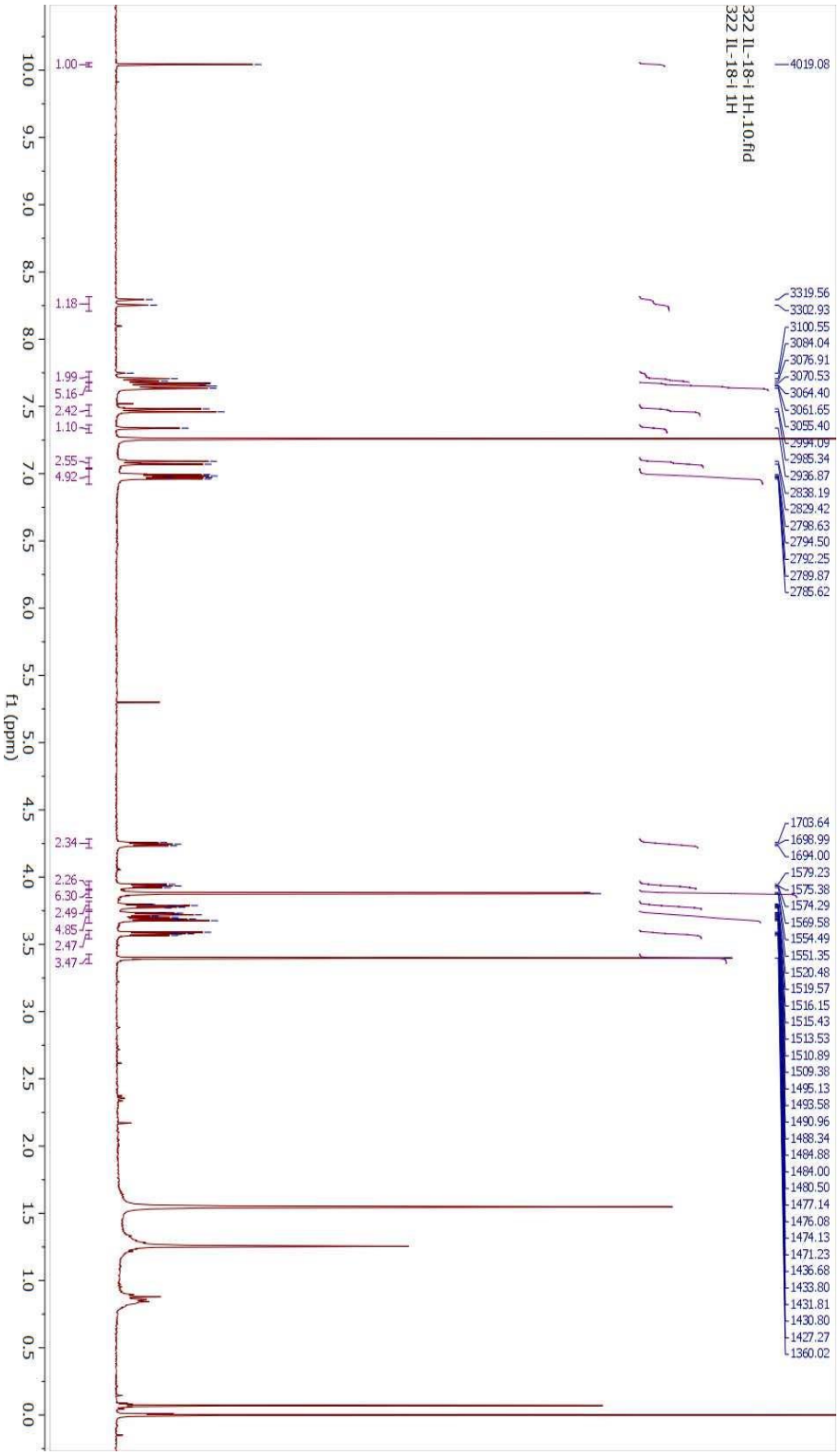

APPENDIX-12. ^{1}H NMR spectrum of molecule 7 ($CDCl_3$, 400 MHz)

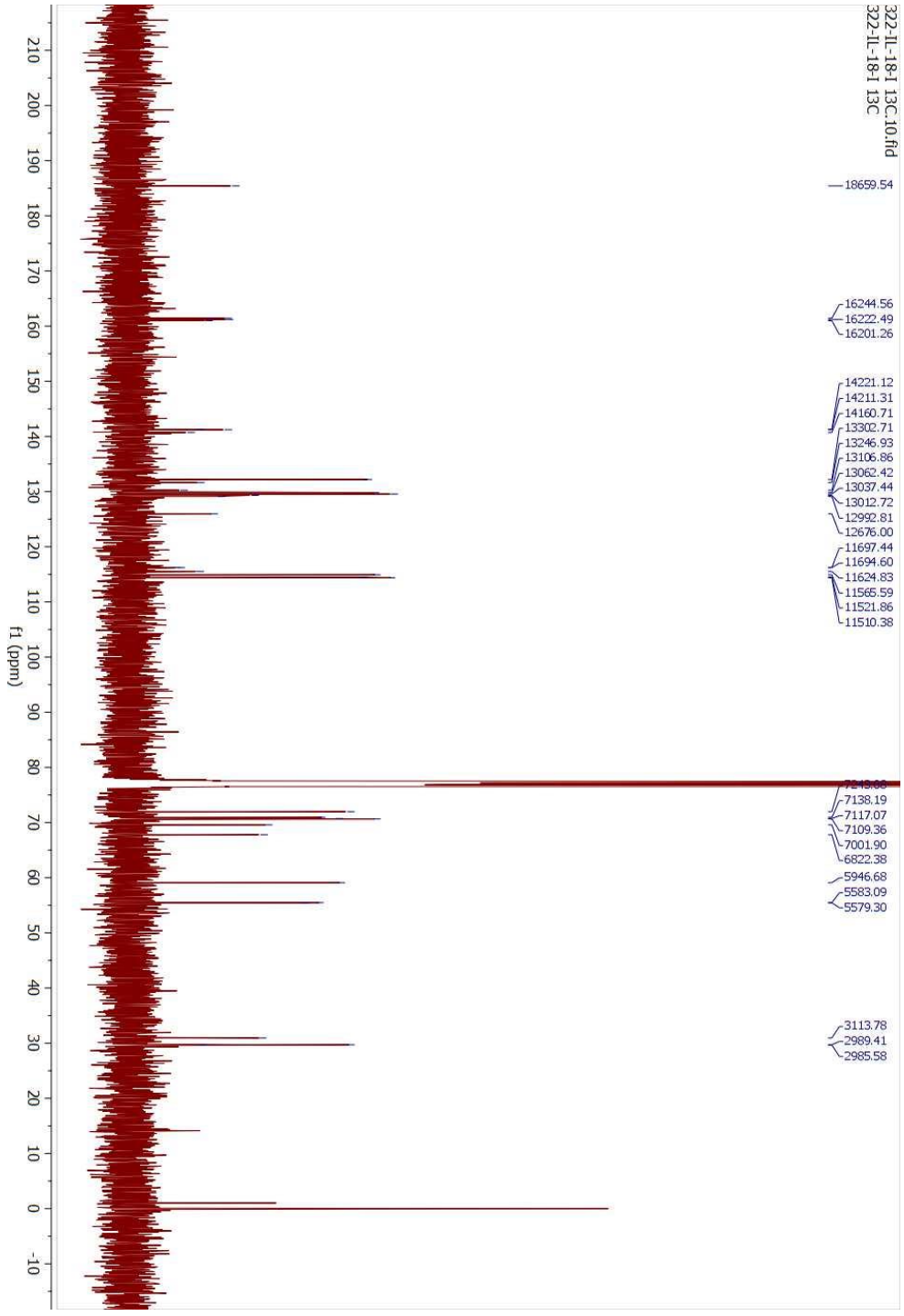

APPENDIX-13. ^{13}C NMR spectrum of molecule 7 ($CDCl_3$, 400 MHz)

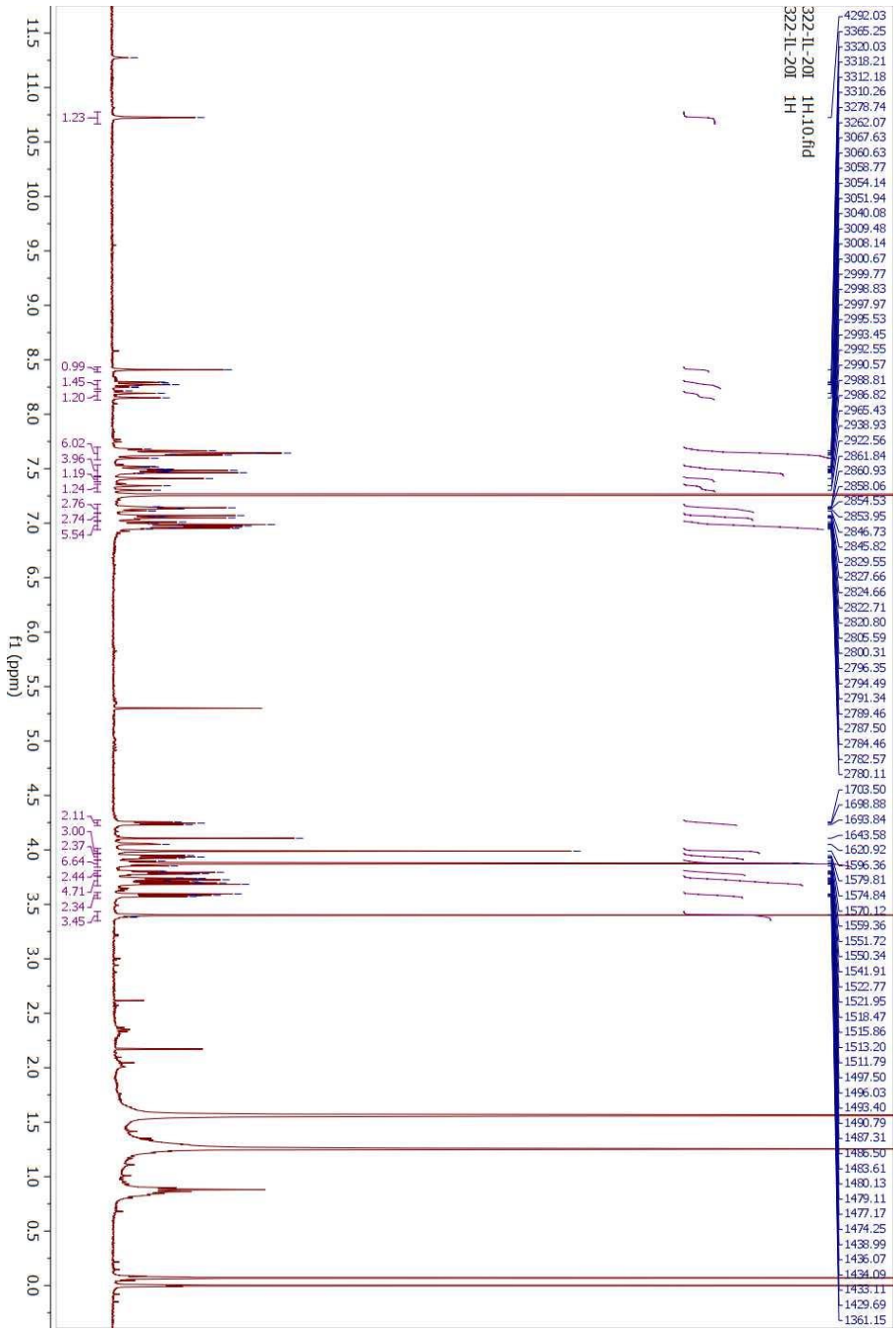

APPENDIX-14. ^{1}H NMR spectrum of molecule PB1 ($CDCl_3$, 400 MHz)

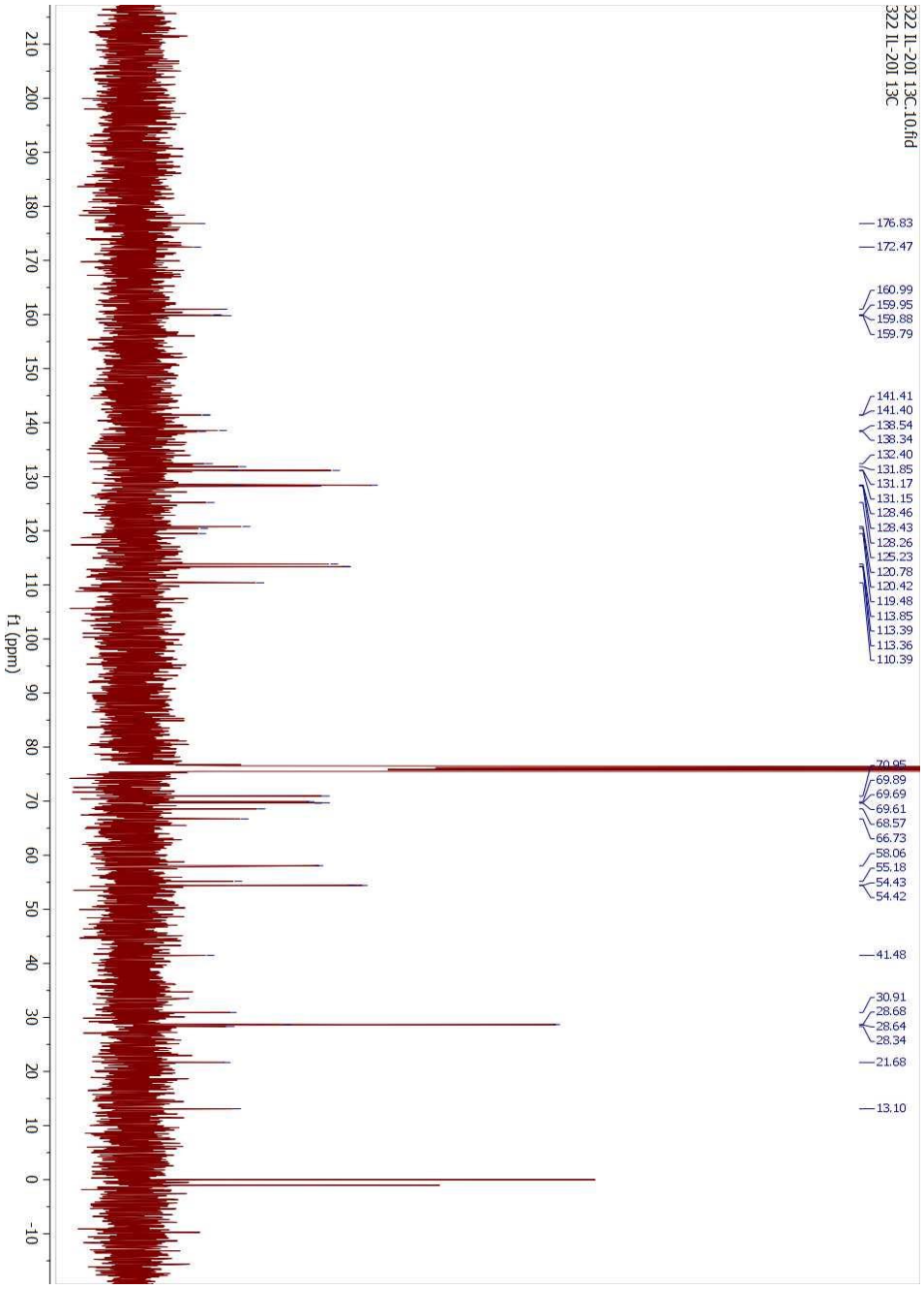

APPENDIX-15. ^{13}C NMR spectrum of molecule PB1 ($CDCl_3$, 400 MHz)

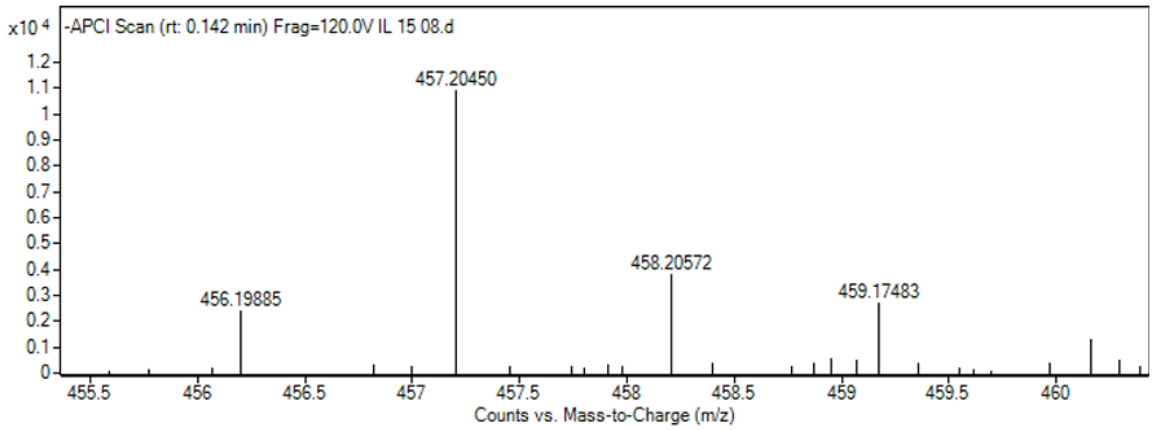

APPENDIX-16. QTOF-LCMS spectrum of molecule 4

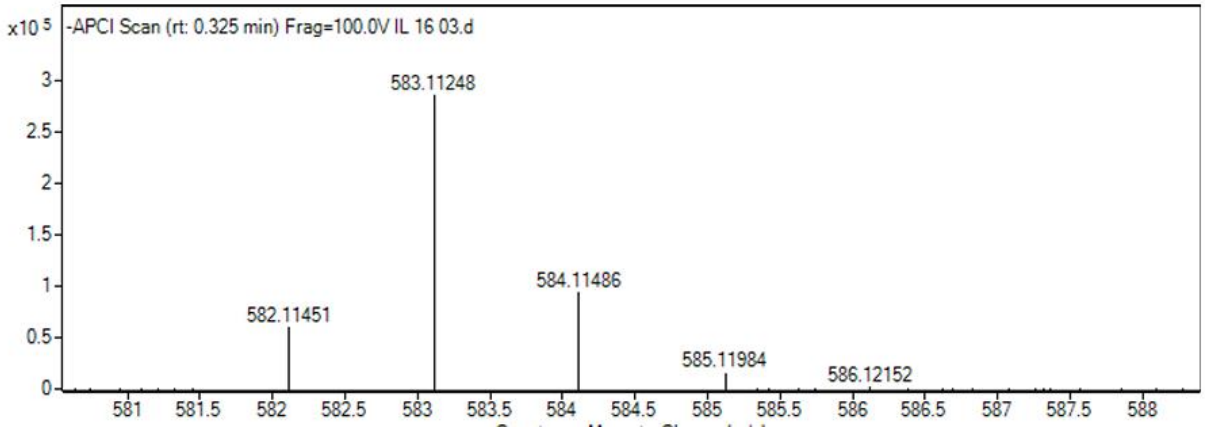

APPENDIX-17. QTOF-LCMS spectrum of molecule 5

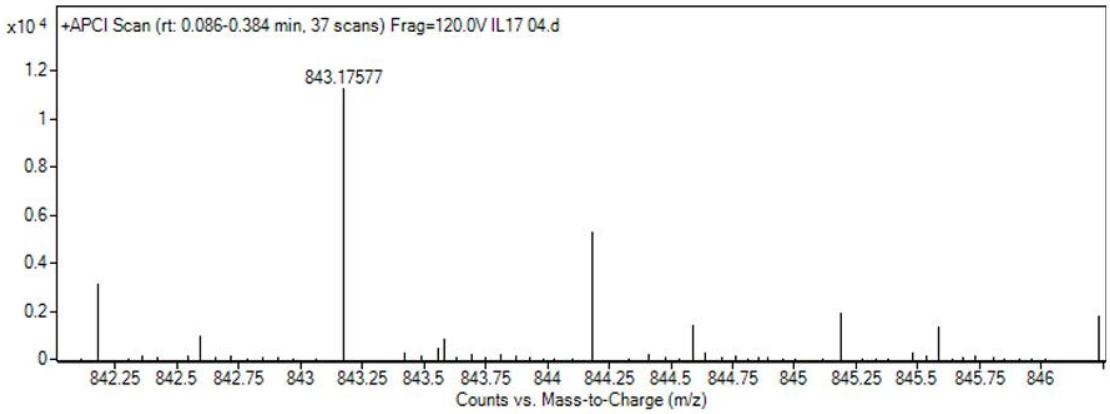

APPENDIX-18. QTOF-LCMS spectrum of molecule 6

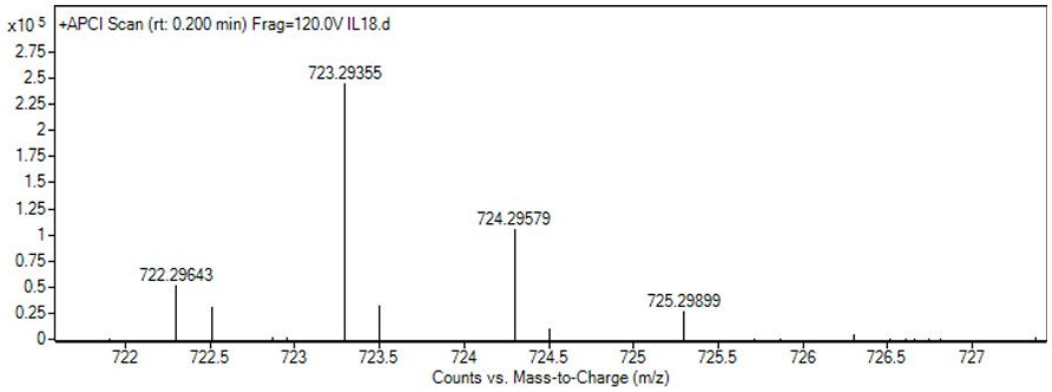

APPENDIX-19. QTOF-LCMS spectrum of molecule 7H

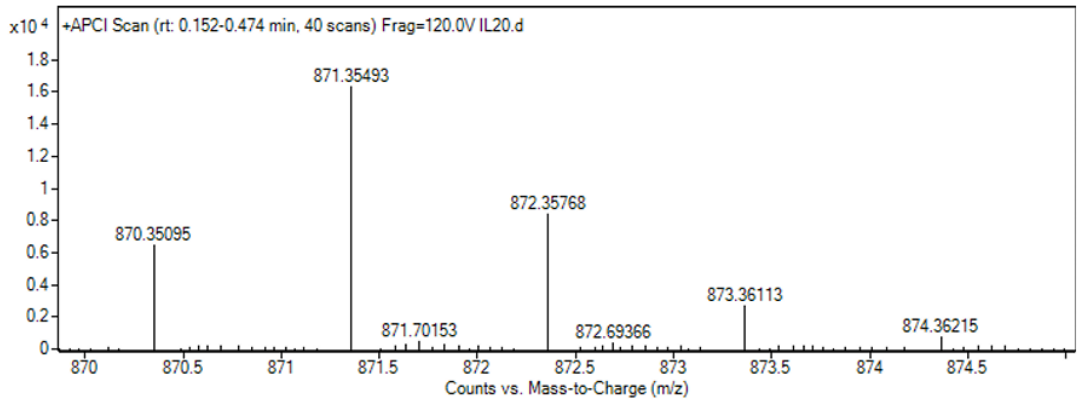

APPENDIX-20. QTOF-LCMS spectrum of PB1H

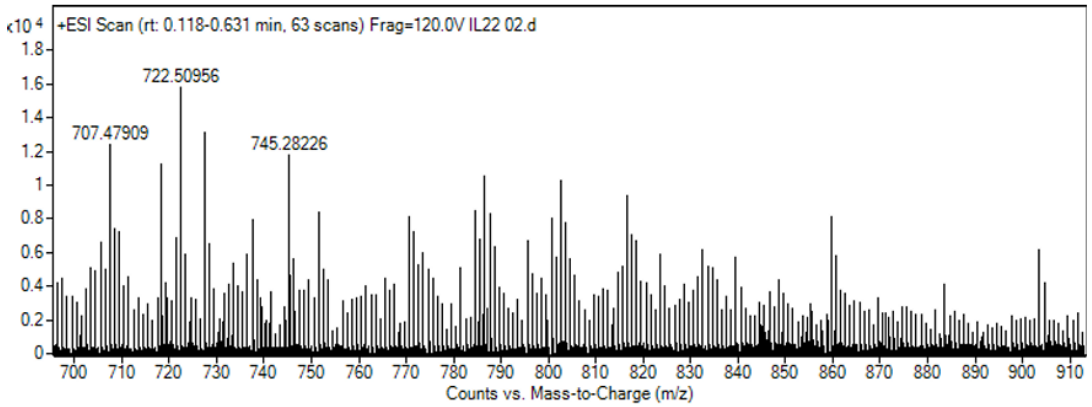

APPENDIX-21. QTOF-LCMS spectrum of PB2H